Electrospun PLLA/SWNT Nanocomposite Fibril for Cartilage Regeneration

A Thesis

Submitted to the Faculty

of

Drexel University

by

Shairali Shiva Rao

in partial fulfillment of the

requirements for the degree

of

Master of Science in Biochemical Engineering

June 2004

Dedications

This thesis is dedicated to my parents B. Shiva Rao and Vimala Rao for their unconditional love and support throughout my life and especially through my education.

Acknowledgements

I would like to extend my gratitude to my mentor and Dr. Frank Ko for his guidance during the course of this work. I wish to thank Dr. Andrzej Fertala, Dr. Richard Cairncross and Dr. Giuseppe Palmese for their time and effort while serving on my committee. The *in vitro* studies in this project were carried out at Thomas Jefferson University in Dr. Andrzej Fertala's laboratory and under his able guidance. His advice and encouragement enabled me to understand various aspects of cells and their interactions and for this input I am extremely grateful. I wish to thank the students and staff of Dr. Fertala's laboratory at Thomas Jefferson University for their help during the *in-vitro* studies. I am also grateful to David von Rohr, Tim Kelley and Dr.Haihui Ye for their invaluable assistance while doing the ESEM, Raman Spectroscopy and TEM respectively. This work would not have been possible without the timely inputs from the students of the Fibrous Research Materials Laboratory --- Milind Gandhi, Hoa Lam, Heejae Yang, Nicholas Titchenal, David Heldt and Dr. Afaf El Aufy. Thanks for the help and also for all the happy hours. Last, but not least, I am extremely grateful to my family for their unconditional love and support throughout my life and especially for having their faith and belief in me.

TABLE OF CONTENTS

LIST OF TABLES

LIST OF FIGURES

ABSTRACT

Electrospun PLLA/SWNT Nanocomposite Fibril
for Cartilage Regeneration
Shairali Shiva Rao
Frank K. Ko, Ph.D.

In this study, Poly-L-Lactic acid has been used as the base polymer to fabricate an electrospun, 3-dimensional, fibrillar scaffold for cartilage regeneration. In the scaffolds, fiber diameters as low as 150nm were obtained with an average of 550nm. The mechanical properties of the scaffold were improved, with a three-fold increase in modulus, by co-electrospinning the reinforcing material (SWNT) with the polymer. The presence and alignment of SWNT in the fibers was confirmed by Raman spectroscopy and TEM respectively. The scaffolds were seeded with human chondrocytes (Cell Applications Inc) and studied for a period of nine weeks. The scaffolds containing SWNT showed no adverse effect on the viability of the cells seeded on them. The cell attachment to the scaffold containing SWNT was increased by incorporating Poly-ε-L-Lysine (ε-PL) in the electrospinning dope. In the presence of ε-PL, seeded chondrocytes tended to maintain a guided growth along the fibrils. Morphology and viability of the chondrocytes seeded on the scaffold were confirmed by ESEM and MTT assay.

CHAPTER 1: BACKGROUND AND SIGNIFICANCE

Over 16 million people in the US suffer from severe joint pain and subsequent dysfunction, such as loss of motion, as a result of injury or osteoarthritis (statistics from American Academy of Orthopedic Surgeons). The most prevalent cause of joint problems is the deterioration of the articular cartilage (AC), a tough, elastic, living tissue that lines the bony surface of joints. The high water content of the AC enables the joint to withstand loads through a wide variety of activities by providing a low friction surface, thus it is a very thin shock absorber[1]. The AC can be damaged either by everyday wear and tear, arthritis, or an injury in a situation of high load. The process of mechanical degeneration of articular cartilage occurs progressively with gradual loss of the normal cartilage structure and function. It starts with the softening of the tissue and then reaches the stage of fragmentation. As the lining of the articular cartilage degrades, the underlying bone (having no protection from the everyday wear and tear) begins to wear out too, leading to osteoarthritis. Thus, mechanical degradation of the articular cartilage would eventually lead to immobility accompanied by a tremendous amount of pain.

The AC has limited natural repair ability and the only living cells in the cartilage tissue (chondrocytes) have a low metabolic and proliferative ability[2]. In the year 1996-1997, about 56% of all musculoskeletal treatments were done at the knee (American Academy of Orthopedic Surgeons), making it very necessary to

develop a treatment of articular cartilage defects especially since permanent repair or regeneration of articular cartilage in synovial, weight-bearing joints (knee, hip) is not achievable using prevalent surgical and non-surgical treatment concepts[3] . Osteoarthritis has been found to be the leading cause of disability and impairment in middle-aged and older individuals[4] leading to significant economic, social, and psychological costs. Each year, osteoarthritis accounts for close to 39 million physician visits and more than 500,000 hospitalizations leading to an expenditure of around 1 billion dollars on cartilage replacement. By the year 2020, arthritis is expected to affect almost 60 million people in the United States and to limit the activity of 11.6 million[3,4].

1.1 Articular Cartilage Structure and Function

Cartilage is an avascular tissue found in several locations in the human body, such as joints, nose, ears and trachea. There are mainly three types of cartilage, namely, hyaline cartilage, fibrocartilage and elastic cartilage. The fibrocartilage contains more collagen while the elastic cartilage contains more elastin. Articular cartilage (AC) is a kind of hyaline cartilage which forms a thin layer on the joint surfaces. The elasticity of the AC enables it to break the force of impact or injury, while its smoothness allows freedom of movement[5]. The presence of synovial fluid (a thick viscous fluid) layer inside the joint enables the articular cartilage to

produce a lubrication mechanism with almost no friction and this lubrication articulates the joint.

The AC varies in thickness according to the shape and location of the articular surface that it lies on. So, wherever the articulating surface is convex, the cartilage is thickest at the center and vice versa for a concave articular surface. The mechanical properties of the AC vary from location to location as well as on basis of age of the person. It is an anisotropic, inhomogeneous and viscoelastic material that exhibits a time-dependent behavior when subjected to a constant load i.e., it has a non-linear stress-strain curve[6]. It provides the joint with a low-friction surface, allowing a smooth, gliding movement, while simultaneously transmitting loads across the joint and dissipating the peak stress on the underlying subchondral bone[3,7].

The articular cartilage is biphasic with two major phases, namely, a fluid phase composed of water and other electrolytes and a solid phase of collagen, proteoglycans and chondrocytes[7]. The major components of the AC are 60% dry weight (dw) (10-20% wet weight) of type II collagen, 20% dw (5-10% wet weight) proteoglycan and 75% wet weight of water. The electrolytes in the interstitial water can be considered as the third phase. The other components of the AC include link protein, biglycan, decorin, types I, V, VI, IX of collagen[5,7,8]. Type II collagen provides the tensile strength through a strong covalent bonding between its fibers while the proteoglycans (PG) provide compressive stiffness

through the fixed negative charges. On the other hand, the AC exhibits a high resistance to fluid flow and can induce a swelling pressure due to the presence of electric charges.

The structural hierarchy of the cartilage tissue is quite complex. In fig.1.1, the schematic in the top left is of the knee joint showing the articular cartilage, tendons and ligaments. The top right schematic in fig.1.1 shows the actual bearing surface of the knee joint, the scale being between 100 microns and 1 cm. The bottom right structure in the schematic is the microstructure of the articular cartilage (.1-100 microns), where the presence of chondrocytes and organization of type II collagen fibrils is clearly seen. At this level of the hierarchy, the organization can be divided into four zones from the top: superficial zone (10-20% of the cartilage thickness), middle zone (60% of the cartilage thickness), deep zone (30% of the cartilage thickness) and the calcified cartilage zone where the cartilage interfaces with the bone at the joint (Fig 1.1,1.2,1.3). The four zones contain different collagen organization as well as different amounts of proteoglycans. The superficial zone contains the highest collagen content (85% dw) and the collagen fibrils are oriented parallel to the joint surface (Fig 1.2). This gives an indication that the superficial zone primarily resists shear stresses at the joint surface. The collagen content decreases in each zone down to the bone, with the middle zone containing 68% dw of collagen.

The cells (chondrocytes) and nuclei are small throughout the cartilage tissue and are elongated and parallel to the surface in the superficial zone, while they tend to be rounded and arranged in columns in the deep zone[5](fig 1.2,1.3). In deeper zones, the chondrocytes are completely surrounded by the extracellular matrix while in the calcified zone; the chondrocytes are branched and eventually cross over to the synovial membrane separating the cartilage from the bone at the joint. Some chondrocytes have cilia that extend from the cell into the ECM and sense the mechanical environment of the cell and are known to modify matrix properties in response to loading[9]. The other two schematics in fig.1.1 show the structure and organization of the collagen and proteoglycans in the vertical section of the articular cartilage[6,7].

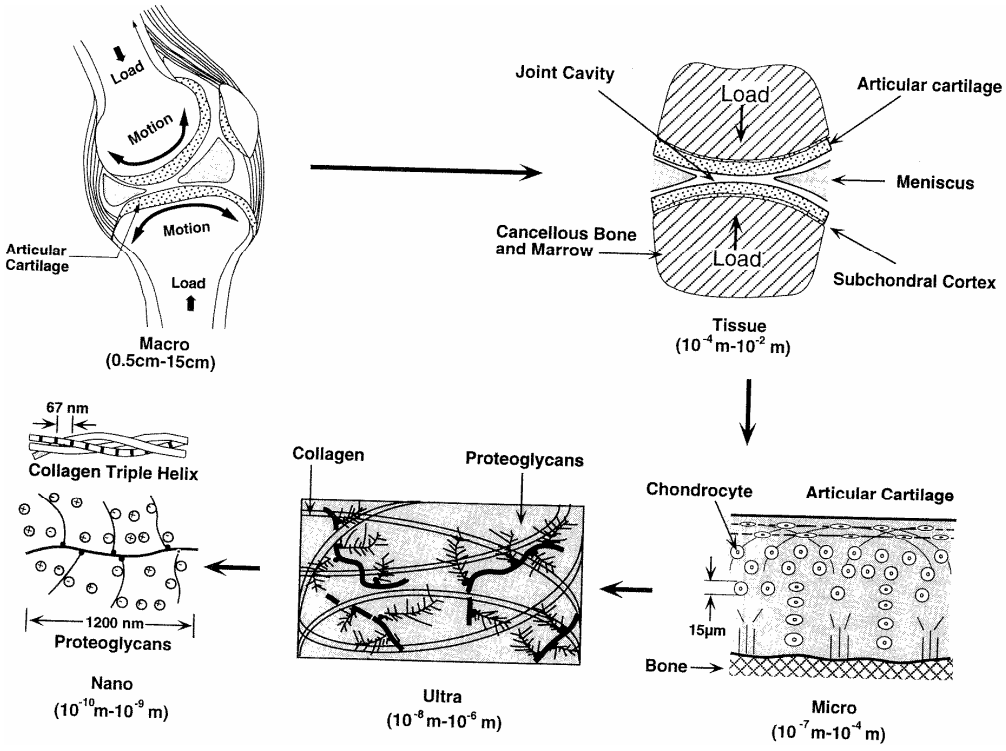

Figure 1.1. Complex structural hierarchy of the articular cartilage[8].

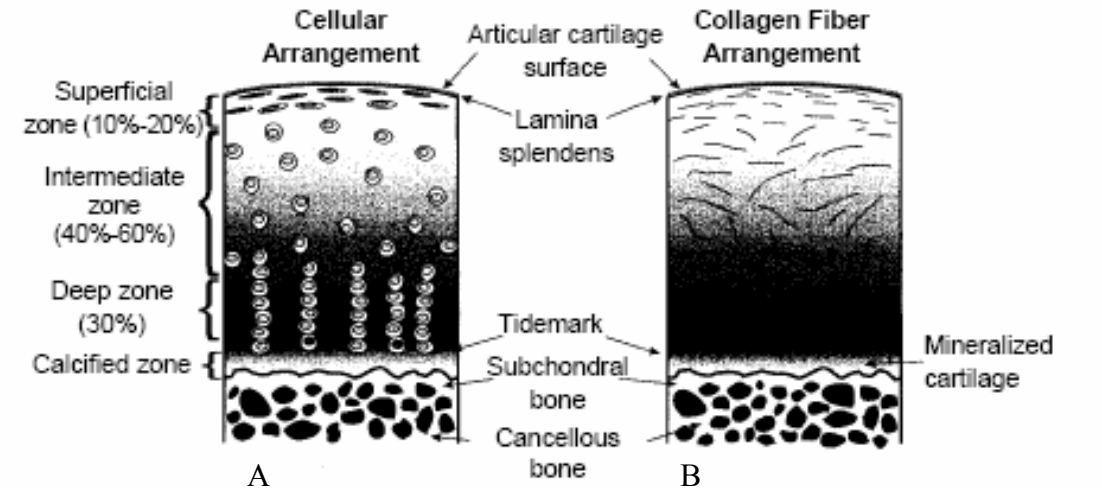

Figure 1.2. A. Zones of cellular organization B. Collagen fibril arrangement in AC[8,10].

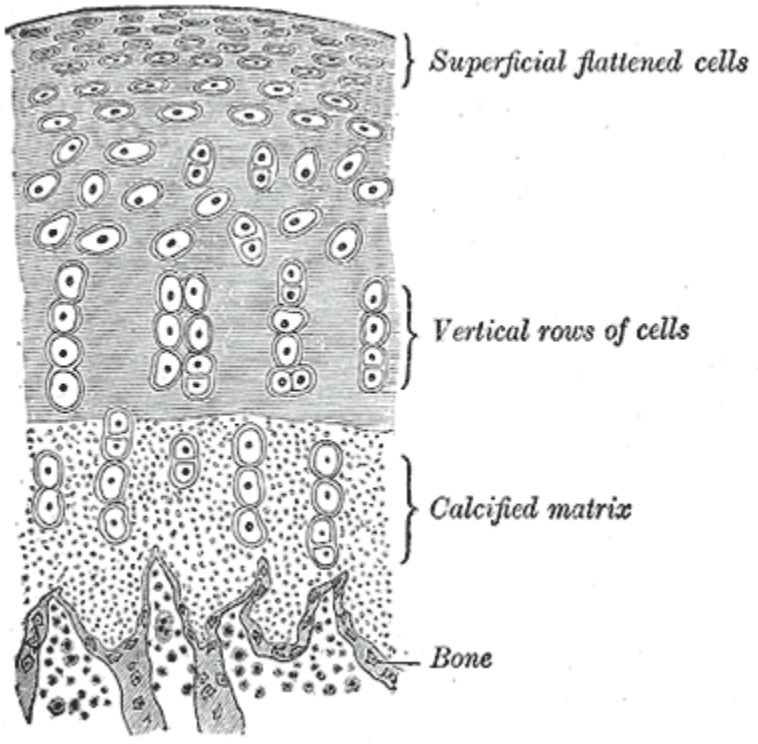

Figure 1.3. Vertical section of the cartilage tissue showing the layers.

The interstitial water is the most abundant component of the AC[11,12]. Of the 60% water present in the AC, 30% of it lies in the intrafibrillar space of the collagen[13]. At physiological pH, the collagen fibril diameter and the amount of water within the collagen are determined by the swelling pressure due to the fixed charge density (FCD) of the proteogylcans. Proteoglycans are composed of 95% polysaccharide and 5% protein. The protein core contains one or more types of glycosaminoglycan (GAG) chains. At least one component of the GAG molecule has a negatively charged sulfate or carboxylate group, so the GAGs tend to repel each other and other anions while attracting cations[10,14]. As the proteogylcans are confined within the collagen matrix, these charges create electrostatic repulsive forces which are responsible for the compressive stiffness of the AC. These repulsion forces are neutralized by the surrounding positive ions present in the fluid. As the rate of loading increases during a compression or pressure gradient (such as walking etc), the fluid is pushed out of the cartilage and the drag forces between the fluid and the matrix increase making it difficult to give out water. During the exclusion of water, there is a higher concentration of ions within the tissue compared to outside the tissue leading to swelling pressures[7,9]. This also increases the electrostatic repulsion. Therefore, the amount of water present in the articular cartilage depends on the concentration of proteoglycans, the organization of the collagen matrix, and the stiffness and strength of the collagen network. Thus, the collagen matrix resists swelling of the cartilage. In the case of osteoarthritis, the collagen matrix is degraded and so the amount of water in the cartilage increases, leading to significant alteration in the mechanical behavior

and properties of the cartilage [7,12,15]. The water is involved in providing many important biomechanical functions of the tissue through binding to the hydrophilic proteoglycans as well as the osmotic swelling phenomenon and relative motion between the interstitial water and the porous matrix.

The AC has no blood supply and the living components of the cartilage, the chondrocytes survive on the nutrients transported through the matrix. The collagen/proteoglycan matrix provides not only the structural framework of the tissue but also forms a fluid compartment for transport of nutrient, waste products, chemical messengers and hormones, to and from the chondrocytes. Small solutes (oxygen, sulfate) are transported via diffusion while large solutes (growth factors) are transported by convection. As the cartilage degrades, the products of degradation are replaced by new components synthesized by the chondrocytes [4,5,7]. So the chondrocytes synthesize proteoglycans as well as collagen.

The stress-strain behavior of the AC is non-linear with the tensile behavior displaying an initial toe region followed by a linear extension. It displays a low tensile strength (1-10 MPa) and a compressive modulus of about 1 MPa. The elastic modulus of articular cartilage is typically 0.3–1.5 MPa[16]. However, *in vivo* peak stresses up to 18 MPa have been measured in the joints during dynamic loads. This vast difference in the peak stresses is due to the relatively low permeability of cartilage. During dynamic loading, the interstitial water cannot be

squeezed out from the tissue, instead, it is pressurized and therefore it is able to support high physiological stresses. Thus, the dynamic stiffness of cartilage may be 10 to 20 times higher than the intrinsic modulus of the matrix itself.

The stress-strain plot associated with the articular cartilage is linear to failure (low yield) (Fig 1.4)[6]. The high weight bearing areas are stiffer than the low weight bearing areas. The AC has a layered structure dependent on the collagen structure and content, with the top-most zone having fibers parallel to the surface, the middle zone having randomly angled fibers (preference toward 45^0) and the bottom-most zone having fibers perpendicular to the surface and crossing over to connect to the calcified tissue (Fig 1.2).

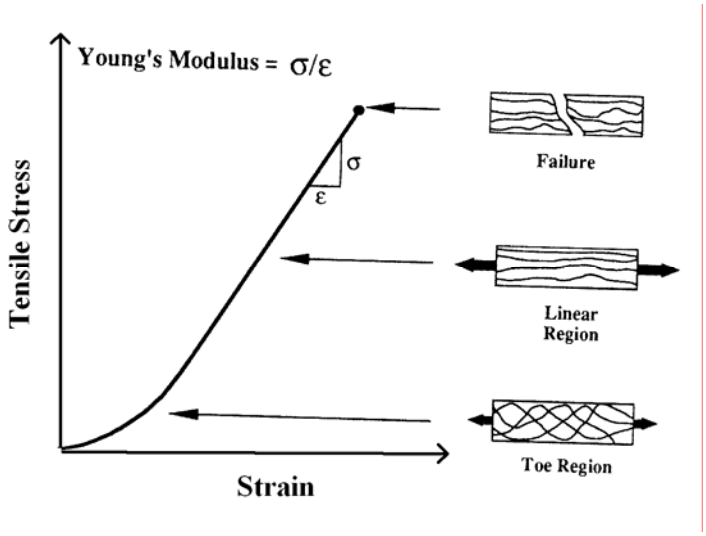

Figure 1.4. Stress-Strain curve for a healthy cartilage

1.2 Techniques for Articular Cartilage Repair

During the course of OA, structural lesions typically develop within the articular cartilage layer. The process of OA is initiated by the loss of proteoglycans from the extracellular matrix and a disruption of the fibrillar collagenous network and all this followed by cell loss[17,18]. The AC has limited natural repair ability because it is avascular and the only living cells in the cartilage tissue (chondrocytes) have a low metabolic and proliferative ability[4,10]. In addition to this, the proteoglycans in the extracellular matrix (ECM) can prevent cell adhesion, further undermining the native repair process[4,19,20]. The spontaneous repair of articular cartilage is thus associated with defects that penetrate the bone and bone marrow spaces, being dependent upon the lesioning of blood vessels, and bleeding. Current techniques for articular cartilage repair include bone marrow stimulation techniques, chondral shaving, laser chondroplasty, abrasion chondroplasty and perichondral and periosteal interposition grafts. Some of these methods are mechanical surgical interventions which involve either removal of the damaged area or inducing a healing process by causing the tissue to bleed. The other methods involve the use of biologics meaning that they seed isolated cells on a designed construct for *in vivo* implantation.

1.2.1 Mechanical Therapeutic Interventions

These therapeutic interventions were developed more than 20 years ago and include bone marrow stimulation techniques (abrasion arthroplasty, drilling, microfracture) and chondral shaving. Bone marrow techniques are based on therapeutically-induced bleeding from the subchondral bone spaces and subsequent blood-clot formation[18]. In the drilling technique, therapeutic holes (2-2.5mm diameter) are drilled into the subchondral bone-marrow spaces underlying regions of damaged articular cartilage and this stimulates a spontaneous repair reaction. The microfracture technique involves generation of very small holes (0.5-1 mm diameter) across the entire articular cartilage lesion site, about 3–4 holes per cm^2. The microfracture technique disturbs the biomechanics of the AC less drastically than the drilling process. Unfortunately, bone marrow techniques produce a tissue that is variable in composition, structure and durability and is mainly fibrocartilage and therefore do not offer a long-term cure. The procedures are not reproducible either and are highly dependent on patient's age as well as severity of arthritic condition[18,21].

Chondral shaving aims at the surgical mechanical removal of diseased chondral tissue, thus making the surface smooth again for proper functioning of the cartilage. This procedure can also be carried out by a laser (laser chondroplasty)[18]. However this procedure have not shown tissue repair for more

than 12 weeks after implantation and is accompanied by cell death and degeneration of the cartilage tissue[22] .

1.2.2 Therapeutic Interventions with Biologics

These techniques include autologous tissue transplantation, allogeneic chondral transplantation as well as tissue engineering. Autologous transplantation includes perichondral and periosteal interposition grafting that produce repair tissue with inadequate mechanical durability and due to immunological constraints, it is very tough to get a graft to match the recipient articular surface[23]. Allogeneic chondral transplantation aims at substituting damaged or lost tissue with healthy articular cartilage, usually derived from cadavers. The main drawback of using tissues from cadavers is bacterial infection, immunological host rejection and the risk of transmission of fatal diseases such as HIV and Hepatitis. Cell-based tissue engineering offers an alternate route for cartilage regeneration as it could provide a transplant material that can meet the in-vivo requirements of the cartilage. Among all the current techniques of cartilage repair, the tissue engineering approach stands out as this approach combines a biodegradable porous scaffold and chondrocytes (cartilage cells) and has proved to be a promising approach for cartilage repair[24].

1.3 Tissue Engineering and Regeneration

"Tissue engineering is the synthesis of new cell-adhesion-specific materials and the development of fabrication methods to process reproducibly three-dimensional synthetic of natural biodegradable polymer scaffolds with tailored chemical and physical properties such as porosity, pore size distribution and connectivity, mechanical properties and rate of degradation."

----------Vacanti and Mikos[25] (1995)

Tissue engineering has been recognized as a promising alternative to donor tissues, which are in short supply. The risk of immunological rejection responses is also vastly reduced. It promises to restore the biologic function lost in the damaged host tissue[26]. Tissue engineering (TE) is the use of a scaffold to provide a specific architecture on which seeded cells can organize themselves and develop into the desired tissue prior to implantation[27]. The technique of tissue engineering involves cell isolation and harvesting, followed by seeding of the scaffold with cells leading to in vitro cell culturing, at the end of which the scaffold is implanted into the patient. The scaffold should provide the initial biomechanical/biochemical profile for the replacement tissue until the cells produce an adequate extracellular matrix. During the formation of the newly generated matrix, the scaffold is either degraded or metabolized, leaving a vital tissue (or organ) that restores or improves the tissue function[11]. While TE is the implantation of *in vitro* seeded matrices, tissue regeneration is the use of acellular

matrices that are implanted into the host and are repopulated in vivo[10,11,28]. Repopulation of acellular and unseeded matrices is still a relatively new area of research and so it is very speculative whether these matrices can be successful in humans[29].

1.4 Material Selection

The most important characteristic to be considered while choosing a material as a scaffold for tissue repair is its compatibility with the environment in which it will be placed *in vivo*. It should be able to adhere to the site of repair when implanted. Under no circumstances, must the material prove to be toxic to the body or generate host rejection response. In addition to this, during the repair process, it should provide the mechanical/chemical/biological properties of the tissue it is aiming to regenerate. The material as well as architecture of the scaffold itself should encourage the original tissue to produce the elements required for its own repair. Another important aspect in the design of a scaffold is the cost of fabrication. This is an important consideration as the scaffold is to be used in vivo and should therefore be affordable to all patients.

As the AC is constantly subjected to a variety of loading conditions, it is essential to analyze the stress experienced at the site of repair before choosing a material for its repair. The material being used to regenerate this tissue should be able to sustain the loads it faces at the site of repair. Therefore, while choosing a material

for the repair of this tissue, the structural complexities as well as stresses experienced at the site have to be analyzed. In addition to this, the architecture of the scaffold should provide sufficient space for the chondrocytes to grow and enough surface area for the cells to attach[30].

Most biological materials like bone, skin and cartilage tend to be composites. To mimic the complexity of the cartilage tissue, it is advisable to use composite biomaterials as they can be tailored to suit any mechanical or physical requirements such as shape, conductivity etc[31]. Synthetic polymeric scaffolds are typically of two kinds --- biodegradable and non-degradable. The biodegradable scaffolds are composed of materials which will eventually break down into molecules which can that be either metabolized or excreted through natural processes of the body and so are used for short-term applications. The non-degradable materials are used for long-term applications such as hip replacements. It is, however, preferable to use biodegradable materials because non-degradable materials tend to wear out with time and these tiny worn out particles prove to be harmful to the body[4,9,11].

Polymeric scaffolds have been used to fill defects as they cover up the injured region and reestablish an articulating surface and during the regeneration period they provide physical and mechanical properties of articular cartilage[7]. As mentioned above, the extracellular matrix of articular cartilage is mostly type II collagen and proteoglycans which form a fibrous mesh. In order to mimic this

environment, the engineered randomly arranged fibrous scaffolds are required to have a morphological structure similar to that of the extracellular matrix. This structure can be provided by fibrous polymer meshes. The advantage of a nanofibrous matrix is that it provides a large surface area for the cells to attach.

For the TE of AC, to date, several types of polymeric scaffolds have been studied both *in vitro* and *in vivo* [32,33,34,35]. These studies have involved the use of synthetic, biodegradable polymers such as poly(glycolic acid) (PGA), poly(lactic acid) (PLA), their copolymer of poly(DL-lactic-co-glycolic acid) (PLGA), as well as natural, biodegradable polymers such as collagen, gelatin, fibrin, and alginate, in the form of sponge, fiber, hybrid mesh[36] and gel. Combinations of synthetic polymers and natural polymers have also been studied for the TE of AC. Both PGA and PLA are approved by the US Food and Drug Administration (FDA) for human clinical use in specific applications. It has been suggested that chondrocytes are more biocompatible with non-woven PLA than non-woven PGA[37]. PLA is a linear, uncrosslinked, resorbable, α-hydroxy polyester (fig. 1.5) that undergoes degradation with uniform mass loss. The hydrolysis of the ester bond in PLA forms lactic acid which is a byproduct of anaerobic metabolism in the body and is eventually excreted from the body as a combination of carbon dioxide and water. PLA is more hydrophobic than PGA due to the presence of a methyl group and as a result, the hydrolysis rate of PLA is slower than that of PGA. The *in vivo* degradation time for PLA is several weeks and this is enough time for the tissue being repaired, to regain its structural integrity and function.

For this reason, Poly-L-Lactic acid (PLLA) has been used as the base polymer in this study.

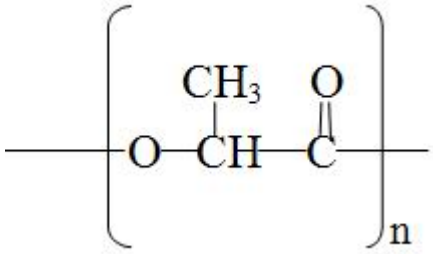

Figure 1.5. Repeating unit of poly-L-Lactic acid.

1.5 Fabrication of Polymeric Scaffolds

After the material of construction is chosen, the next step in the sequence is fabricating the scaffold. To date, there are several fabrication techniques available, such as, gel casting, solution casting, solvent casting, gas saturation, lyophilization, emulsion freeze-drying method, solvent casting[38], membrane lamination[39], melt molding, electrospinning, extrusion of the polymer into fibers and processing them into a fibrous mesh[40], coating a polymer with another (eg, PGA with PLLA) followed by heating to bond the fibers and to maintain a structure which would improve its mechanical properties. Placing the porous scaffold in a solid, degradable framework (matrix) is another approach[3,4]. The addition of short fibers to a porous, resorbable scaffold, using the proper fabrication technique results in an orientation of the fibers.

Solvent casting of a mixture of polymer and salt crystallites of well-controlled size is a well defined method of producing the necessary porous structure. After the solvent is removed, the salt is leached out with water and this results in voids that are the same size and shape of the crystallites and the size of the voids may be varied continuously. Pore sizes up to 700 μm have been produced[7,41,42]. However, the disadvantage of solvent casting techniques is that it cannot produce a three-dimensional scaffold as it can produce only wafer thin slices[5].

Solution casting of a 50/50 composite copolymer of PLGA involves dissolving the polymer in an organic solvent such as acetone and then precipitating in ethanol. The resulting precipitate is then packed into Teflon molds, placed in a vacuum, and subjected to a specific temperature range. However, the initial porosity of these scaffolds was limited to 40–50%[6].

A gel casting technique has also been used to produce microporous PLGA scaffolds. This involves dissolving the polymer in a solvent (acetone), pouring the solution into a mold and then allowing it to gel. The gel is then extracted and processed through multiple stages of solvent exchanges (mixtures of acetone, ethanol, water) to produce a microporous, solid implant. Bioactive factors may be incorporated into these implants by adding them to the starting solution. The advantage of gel casting with the use of bioactive agents is that the low heat

(<45°C) used in this technique has less likelihood of denaturing the bioactive agents[43].

Electrospinning of a polymer solution to form a fibrous scaffold involves the dissolving of a single polymer or a combination of polymers in a solvent and subjecting this solution to an electric field[44]. The solvent evaporates during its flow through the electric field and dry polymeric fibers are collected. The matrix formed as a result of this is a 3-dimensional, highly porous, fibrous and random structure. Reinforcing materials such as carbon nanotubes (CNT) can also be incorporated in such a matrix by co-electrospinning[45].

CHAPTER 2. HYPOTHESIS AND SPECIFC AIM

This chapter details the basis of this study and outlines the hypothesis as well as aims of this study. The explanations of why this study was undertaken have also been detailed.

2.1 Hypothesis

2.1.1 Hypothesis #1: Incorporation of SWNT in the Polymeric Scaffold Will Improve its Mechanical and Conductive Properties.

The physical properties of a matrix are an integral part of its design. This is more apparent in the design of implants to be used for load bearing parts of the body. The articular cartilage is a tissue that bears load several times the body weight. A damaged cartilage tissue loses most of its functionality and as the cartilage undergoes a variety of stresses, it is imperative for the scaffold being used for its repair to provide the structural integrity during the regeneration process. Collagen is piezoelectric which means that when a force is applied to it, an electric potential is generated. Collagen conducts current mainly by negative charges while the mineral crystals of the bone close to the collagen conduct current by means of positive charges. Both collagen and bone are semi-conductors, and at their junction, current flows easily in only one direction. There is speculation that the forces on bones generated the potentials by piezoelectric effect and that the currents generated at the junctions of collagen-bone, induces and controls bone growth. The currents produced are proportional to stress supplied, so increased mechanical bone stress results in increased growth[46,]. A healthy cartilage tissue

comprises 70% water and this water is held in the tissue by the conductivity of the structure. The water carries off most of the compressive loads at the cartilage. Therefore, conductivity is a required property of cartilage scaffolds as it is necessary to stimulate cell growth in addition to aiding the structure to retain water inside the tissue to bear the compressive stresses at that location. SWNTs have been known to have exceptional mechanical (elastic modulus 1-5TPa and strength 30-180GPa) and conductive properties (6000 S/cm²) and therefore its incorporation in the scaffold is expected to improve the physical properties of the scaffold itself.

2.1.2 Hypothesis #2: Electrostatic Charge During the Electrospinning Process Will Align Carbon Nanotubes Along Fiber Orientation.

In order to capitalize in on the unique properties of SWNTs, they have to be organized into well aligned assemblies. In the polymeric solution, the SWNTs are well dispersed but are randomly oriented. SWNTs can be aligned during electrospinning due to three mechanisms, namely, flow induced orientation, charge induced orientation and confinement. Like logs flowing down a river, SWNTs tend to get carried along with the flow of the polymeric solution and eventually align themselves along the flow orientation (Fig. 2.1). During the flow through the electric field in the electrospinning process, the field too induces the SWNTs to flow with the current and align along the fiber. In addition to this, for the SWNTs to be included within the fiber, as the fabricated fibers are less than a

micron, the micron long nanotubes have to be along the fiber orientation[2] (Fig. 2.2).

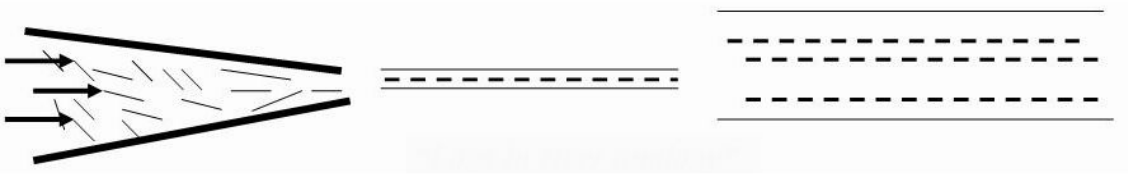

Figure 2.1. Alignment of SWNTs along the polymeric solution flow.

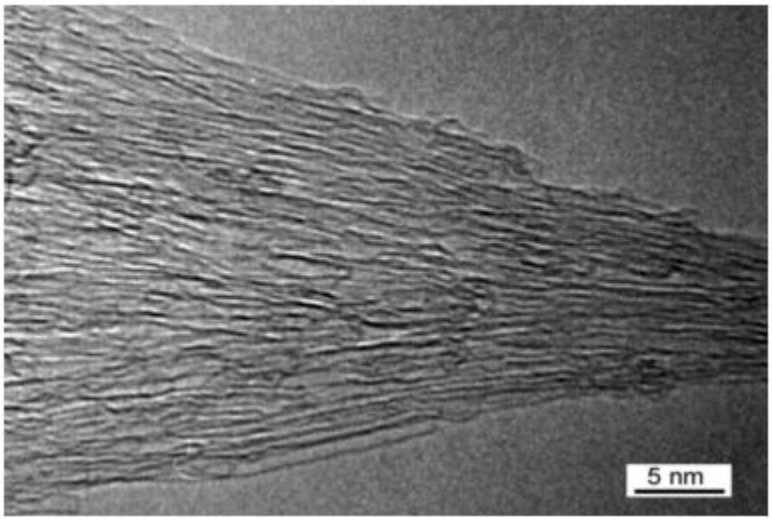

Figure 2.2. TEM image of SWNTs aligned along the polymeric fibril[2]

2.1.3 Hypothesis #3: Nanofibrous Structure Will Aid Cell Attachment and Proliferation.

As the electrospun matrix is three dimensional, and is coated with collagen it is expected to mimic the *in vivo* environment of cartilage cells. The three dimensional structure of the scaffold will aid in the transport of nutrients and will also provide the frame-work for the cell extensions to attach to and proliferate along. The advantage of a nanofibrous matrix is that it provides a large surface area for the cells to attach as well as a high porosity and a wide range of pore size distribution. The tensile stresses acting on the articulating surface of the cartilage are fended off by the tangential orientation of the collagen in their matrix. The fibrous structure proposed in this study is also expected to be along the tangential orientation of the articulating surface *in vivo*. Together, the unique architecture and composition of the matrix is expected to improve cell attachment and proliferation.

2.1.4 Hypothesis #4: Poly-ε-L-Lysine Will Improve Attachment of Chondrocytes to Scaffolds Containing SWNT.

Lysine is a positively charged amino acid. It is an essential amino acid (not produced in the body) that ensures adequate absorption of calcium, helps form collagen, aids in the production of antibodies, hormones and enzymes. Poly-ε-L-Lysine (ε-PL) is a highly positively charged polymer chain of lysine and is commonly used as a coating agent to promote cell adhesion in cultures. The free NH_2 group of ε-PL (fig 2.3) is expected to covalently bond with the collagen

coated on the electrospun matrix and the positive charge of lysine is expected to attract the negatively charged chondrocytes. Thus, inclusion of ε-PL in the fibers is expected to result in improved attachment of chondrocytes to the three dimensional matrices. A recent study has shown that functionalizing of SWNT with an amine group significantly improves cell attachment and proliferation on a construct containing SWNT[47]. Therefore, in our study, ε-PL has been incorporated into the scaffold in order to functionalize the SWNT and improve cell attachment and proliferation on the scaffold.

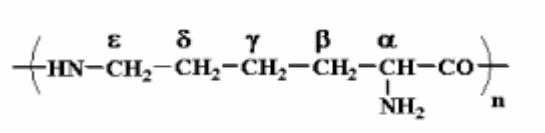

Figure 2.3. Structure of Poly-ε-L-Lysine

2.2 Specific Aim

In order to prove the hypothesis proposed, systematic evaluation of the scaffold and its subsequent interaction with chondrocytes has to be carried out. For systematic evaluation, several techniques have been used for characterization. To this effect, the following specific aims have been established for this project.

2.2.1 Specific Aim #1: Co-electrospin PLLA with SWNT and Test Mechanical and Electrical Properties

It has been demonstrated by Ko *et al*. that co-electrospinning provides an excellent method for aligning CNT in polymer fibril matrix[45,48]. Co-electrospinning is the process in which two or more materials are dissolved or dispersed in the same solvent and electrospun. In this study, Poly-L-lactic acid will be dissolved in a solvent while SWNT will be uniformly dispersed in the same solvent (separately) and mixed with the PLLA solution. This PLLA-SWNT solution will be electrospun to fabricate a three dimensional scaffold. This scaffold will be tested to determine its strength by measuring its elastic modulus using the Kawabata microtensile machine. The conductivity of the scaffold will be determined using the four-probe test. A PLLA nanofiber scaffold containing 0% SWNT will be used as the control group.

2.2.2 Specific Aim #2: Disperse SWNT in PLLA and Characterize the Scaffolds Using TEM and Raman Spectroscopy

The key to the aligning of SWNT along the fiber orientation lies in the uniform dispersion of the SWNT in the polymeric solution. So, the SWNTs will be uniformly dispersed for over a day by sonication and will then be imaged using transmission electron microscopy (TEM) to view the orientation of the SWNTs as well as to study the surface morphology of the fibers. Raman spectroscopy will be used to detect the presence of SWNT inside the fibers.

2.2.3 Specific Aim #3: *In vitro* Study with Human Chondrocytes

The successful implantation of scaffolds *in vivo* is dependent on its architecture and ability to mimic the tissue being repaired within the living system. PLLA is a recognized biocompatible material and SWNT comprise of just carbon and as carbon is the major element in the human body, the PLLA/SWNT scaffold should not be non-toxic to the human body. The scaffolds being studied will be seeded with human chondrocytes and studied over a period of nine weeks. After the cell seeding, at various time points, images of the topography of the scaffold will be studied to gauge cell attachment, inter-cellular bridges and size/shape of cells. The *in vitro* study is expected to reveal a quantitative analysis of cell growth and attachment. A quantitative analysis, MTT (3,[4,5-dimethylthiazol-2-yl]-2,5-diphenyltetrazolium bromide) assay, will be used as evidence of the viability of the cells on the scaffold. This assay quantitatively measures a biochemical product secreted only by viable/living cells.

2.2.4 Specific Aim #4: Co-electrospin PLLA, SWNT and Poly-ε-L-Lysine and Conduct *In vitro* Study with Human Chondrocytes

PLLA and ε-PL will be dissolved in a solvent and SWNT will be dispersed in the same and mixed with the polymeric solution. This solution will then be electrospun to fabricate a three-dimensional fibrous matrix. Human chondrocytes will be seeded on this scaffold and studied over a period of nine weeks. They will be imaged at the various time points to gauge cell attachment and proliferation. The MTT assay will be carried out to quantitatively gauge the viability of cells on

this scaffold. The control group for this study will be a PLLA/ ε-PL scaffold fabricated by electrospinning and seeded with human chondrocytes.

CHAPTER 3: LITERATURE REVIEW

3.1. Synthetic Polymers for Cartilage Regeneration

Several types of materials have been studied as a possible scaffold for the regeneration of articular cartilage. These include biologically derived materials such as collagen, gelatin, fibrin, agarose, chitosan, synthetic polymers, hydrogels, etc. The synthetic polymers fall into the major categories of non-degradable and degradable polymers, as mentioned earlier in section 1.4. Non-degradable poly(vinyl alcohol) (PVA) was the one of the first polymers to be studied as an articular cartilage.

Ko[49] et al compared the results of cell culture on microspheres, electrospun nanofibrous scaffolds and 3-dimensional braided structures (Fig 3.1).

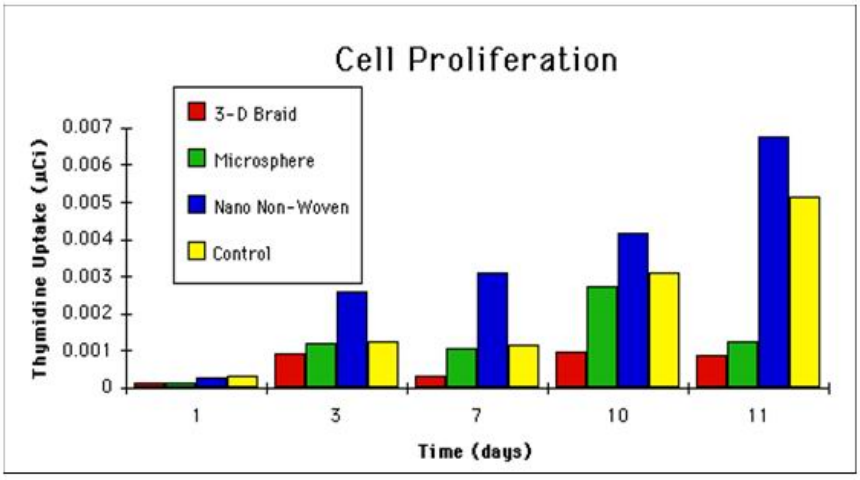

Figure 3.1. Cell proliferation on (A) 3-D braid, (B) microspheres, (C) Non-woven nanofibrous structure and (D) control.

Their study showed that the cell proliferation was highest for the nanofibrous structure and least for the braided structure.

Ma and Langer[50] studied the mechanical properties of non-woven poly-glycolic acid (PGA) disks that had been engineered for cartilage replacement for a period of 25 weeks (fig 3.2). The fibers in the disk had lengths between 50-65 mm and diameters of 15 microns. Their study revealed that the modulus of the disk improved between week 12 and week 20 and upon reaching a numerical value approximately 40% of the natural cartilage modulus, remained constant thereafter. Thus it was concluded that modulus of the engineered scaffold would not approach the numerical value for that of a healthy cartilage upon extended in vitro culturing.

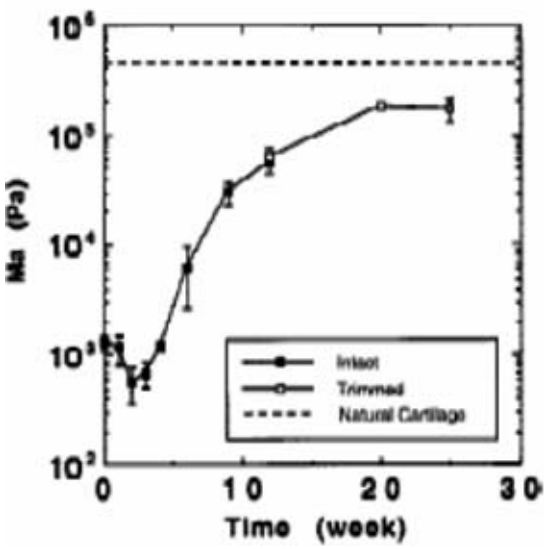

Figure 3.2. Modulus of engineered cartilage versus natural cartilage.

Li et al fabricated a novel 3-dimensional poly(D,L-lactide-co-glycolide) (PLGA) structure by electrospinning for use in tissue engineering[51]. The PLGA fibers in the electrospun scaffold ranged from 500 to 800 nm in diameter (similar to the extracellular matrix (ECM) of natural tissues). The scaffold possessed high porosity with a wide range of pore diameters in addition to improved mechanical properties. These characteristics meet the essential design criteria of an ideal engineered scaffold. The scaffolds were seeded with mouse fibroblasts and studied for a period of 10 days. The SEM images obtained on the 3rd day and 7th day (figure 3.3) of the study clearly indicated that this type of electrospun scaffold with random fibers facilitated cell attachment and guided proliferation along the fibrils. The cells also tended to maintain their phenotypic shape. They concluded that the mechanical properties of this scaffold were suitable for soft tissue regeneration such as cartilage and skin.

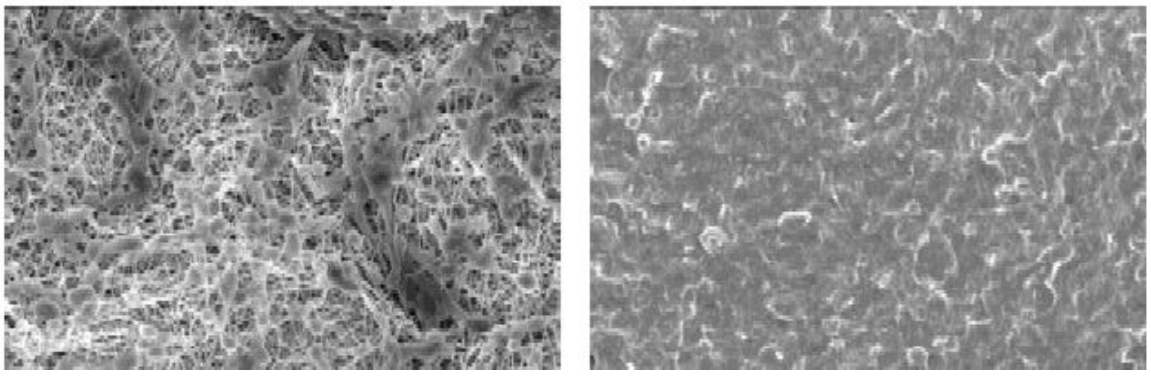

A B

Figure 3.3. SEM image of scaffold seeded with mouse fibroblasts after (A) 3 days and (B) 7 days of cell culture.

Riesle et al tried to determine whether engineered cartilage contains a functional collagen network in vitro[52]. They analyzed polymer-chondrocyte constructs (scaffolds) for 6 weeks of culturing in terms of the composition and structure of collagen. They found that the proportion of the collagen types II, IX, and X as well as collagen network organization, density, and fiber diameters in the engineered cartilage were not very different from that of the natural bovine articular cartilage (fig 3.4). However, the amount of total collagen in engineered cartilage after 6 weeks of cultivation was much lower (57%) than that in natural bovine articular cartilage. Thus, their work indicated that differentiated chondrocytes seeded on scaffolds are able to form a collagen matrix in vitro and produce a tissue similar to natural articular cartilage, but the mechanical properties of the engineered cartilage are not close to that of the natural tissue.

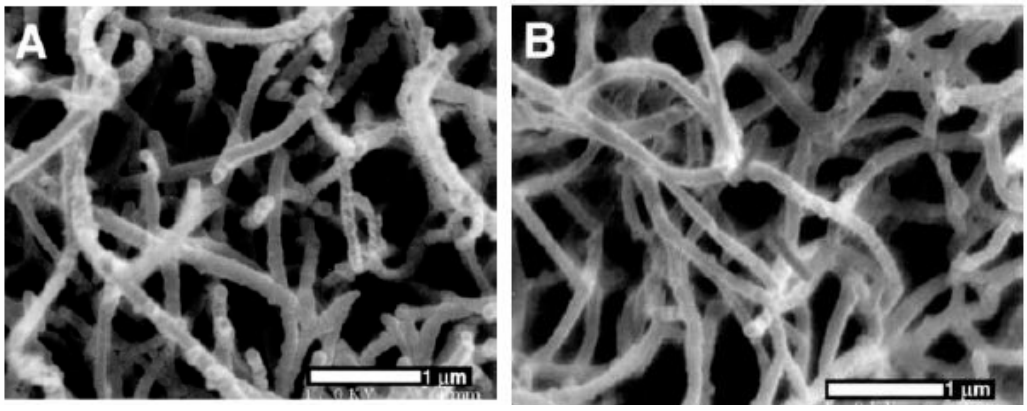

Figure 3.4. SEM images of collagen fibrils. (**A**) 10-day construct and (**B**) natural bovine calf.

Sato et al evaluated the use of a PLLA-collagen hybrid sponge (figure 3.5), with subsequent animal tests, as a suitable scaffold for cartilage repair[53]. Isolated bovine chondrocytes were seeded on this sponge and implanted in mice and studied over 8 weeks. They observed that throughout the *in vivo* cartilaginous tissue homogeneously and abundantly distributed in the hybrid sponge versus the control sponges of PLLA and collagen separately. The found that the hybrid sponge and the PLLA sponge maintained their original shape while the collagen sponge collapsed. They concluded that the hybridization of PLLA and collagen had led to the increase in the hydrophilicity of the scaffold, therefore allowing it to facilitate cell seeding as well as formation of homogenous cartilaginous tissue.

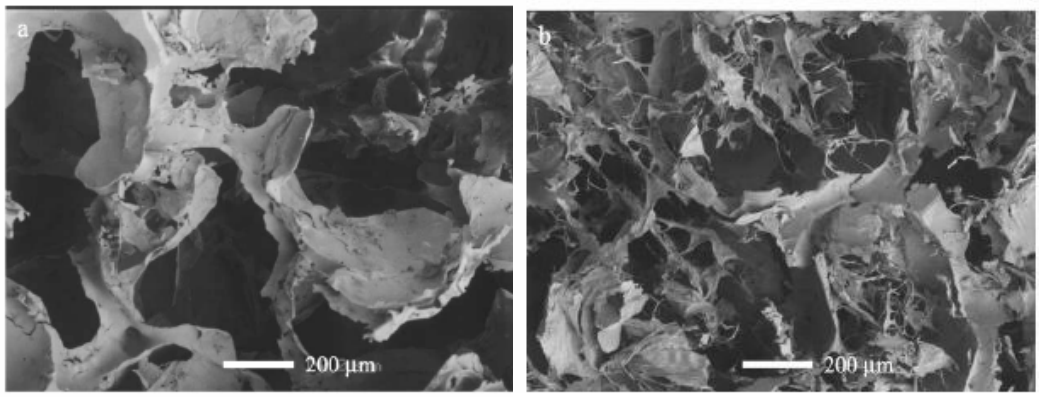

A B

Figure 3.5. SEM images of (A) PLLA sponge and (B) PLLA– collagen sponge.

3.2. Single Walled Carbon Nanotubes

Carbon nanotubes have excellent mechanical and electrical properties[54,55]. Due to their unique properties, SWNTs have been used for several applications such as nanotube tips for scanning probe microscopes[56], very small electronic devices[57] and biomedical applications[58] etc.

Carbon nanotubes have diameters in the range of a few nanometers and lengths of about a few microns. They can be multi-walled (MWNT) or single-walled (SWNT). Compared to conventional carbon fibers, carbon nanotubes have a much higher elastic modulus which is approximately 1-2TPa[59]. SWNTs are known to have better overall properties than MWNTs. SWNT were first synthesized in 1993 by two independent groups[60,61] and they normally tend to be looped[62]. Depending on their structures, SWNTs can be metallic, semimetallic, or semiconducting[63].

The one application of SWNTs that is beginning to receive more attention is the fabrication of polymer-SWNT nanocomposites[64,65,66,67,68]. Incorporation of carbon nanotubes into polymer matrices has been known to significantly toughen the matrix[69,70]. The remarkable mechanical properties of SWNTs make them ideal reinforcements in lightweight polymer composites.

Mickelson studies[71] displayed the Raman spectrum for pure SWNTs (fig 3.6). This spectrum clearly shows the radial breathing mode of SWNT in the wave

number region of 170-190 cm-1 while the stretching mode can be seen around 1580 cm^{-1} corresponding to the sp^2 hybridization of carbon.

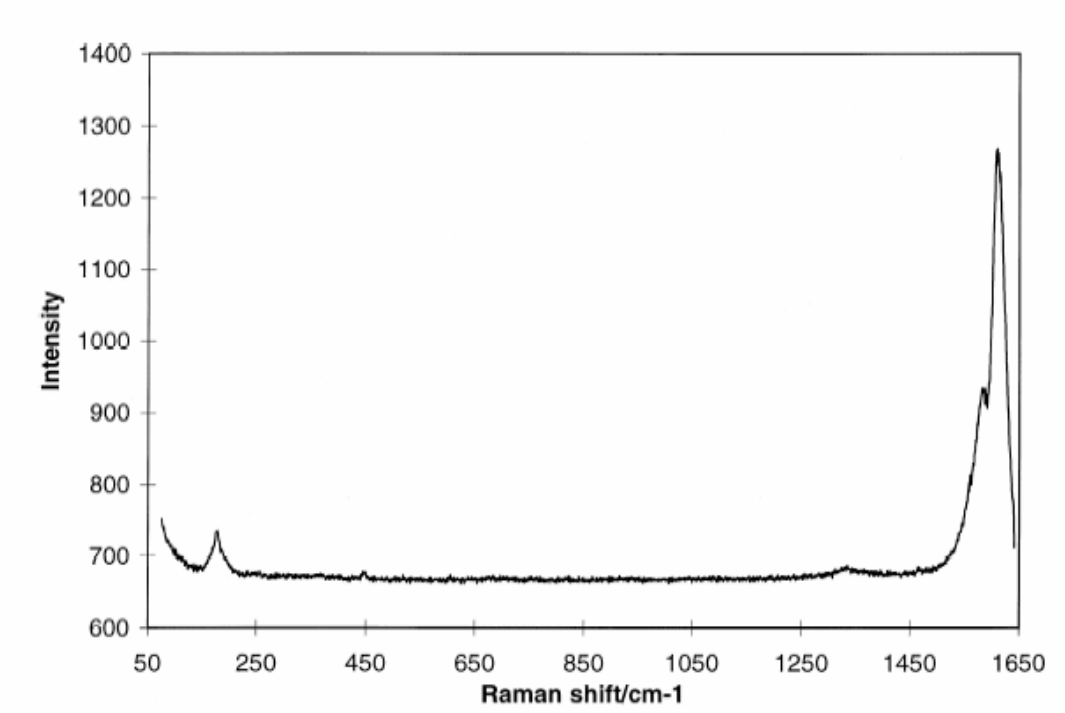

Figure 3.6. Raman spectrum of pure SWNT.

Mccarthy[72], on the other hand, used Raman spectroscopy to study the interaction between SWNT and a conjugated polymer, poly(*m*-phenylenevinylene*co*-2,5-dioctyloxy-*p*-phenylenevinylene PmPV. The spectrum for SWNTs also shows the radial breathing mode and stretching mode (fig 3.7).

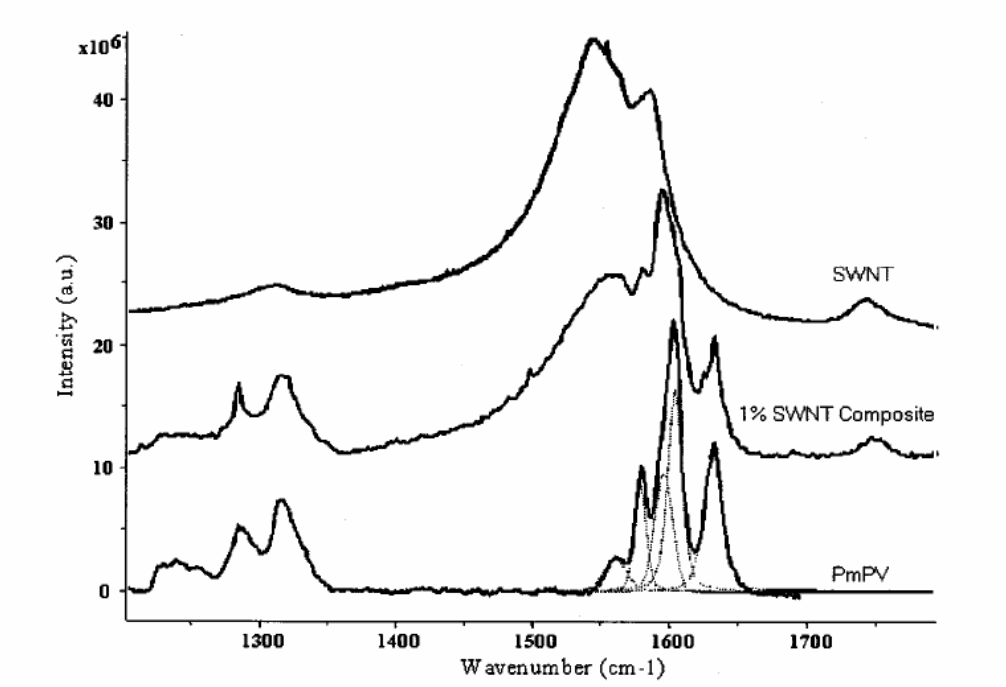

Figure 3.7. Raman spectrum of PmPV-SWNT composite, with PmPV and SWNT spectra for comparison.

A recent study by Nimmagadda and McFetridge assessed the biocompatibility of SWNT for tissue engineering purposes[73]. They seeded fibroblasts on three preparations of SWNT, namely, purchased SWNT, purified SWNT and glucosamine functionalized SWNT. They compared the cell proliferation and cell viability on a range of concentrations (.001-1% w/vol) of SWNT. Their study revealed an inverse relationship between SWNT concentration and cell viability. The cell viability was maximum on the preparation of SWNT functionalized by glucosamine in the concentration range of 0.001-0.0625%. This high viability was attributed to the hydrophilicity of the glucosamine.

Supronowicz[10] et al demonstrated that a nanocomposite blend of PLA and multi-walled carbon nanotubes (MWNT) can be used to electrically stimulate osteoblast cells. They fabricated a nonporous PLA/MWNT disk that was used as a subtrate to expose the cells to an alternating current stimulation. They found the resistivity of the 80/20% w/w composite to be 0.2 Ω-m, therefore, the conductivity was 0.05 $\Omega^{-1}cm^{-1}$. The osteoblast proliferation significantly increased (by 46%) on this composite (fig 3.8). After 21 days of culturing, the osteoblasts had produced almost 307% more calcium under electrical stimulation than without (fig 3.9). Hence, this study suggested an alternate method to enhance osteoblast functionality.

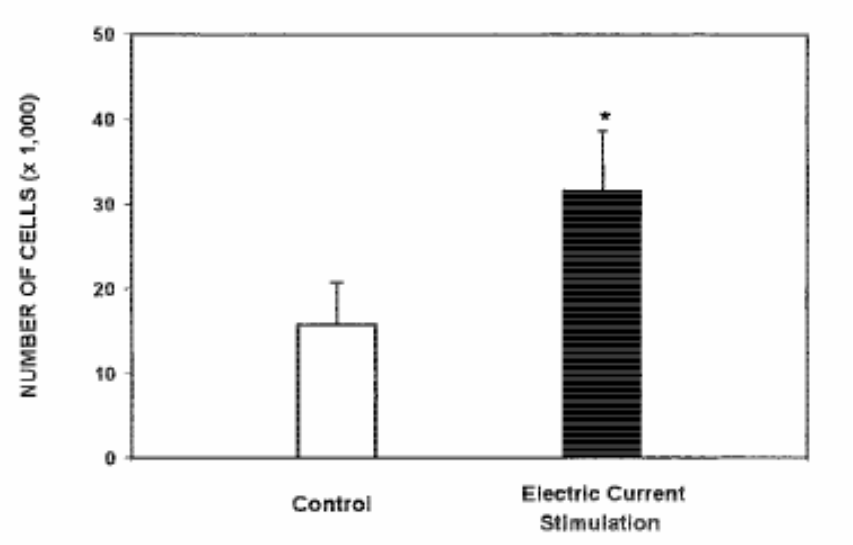

Figure 3.8. Osteoblast proliferation under electrical stimulation versus without electrical stimulation.

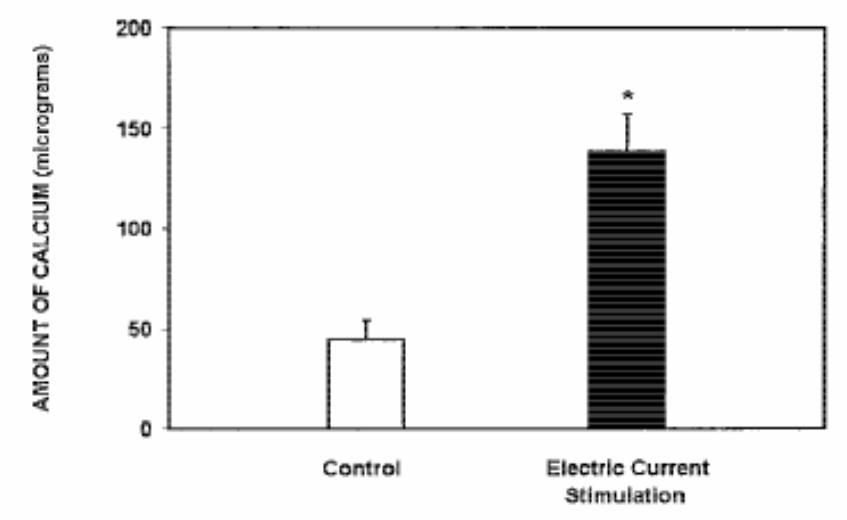

Figure 3.9. Calcium content in osteoblast cultures exposed to electrical stimulation versus without electrical stimulation.

3.3. Electrospinning

Since the initial patent by Formhals[74], electrospinning has been used to fabricate several fibrous, non-woven structures in the nano-scale. Fiber diameters ranging from 10 microns to 20nm have been reported[75,76]. Presently, it is widely used to fabricate polymeric nanofibers for various applications. Electrospinning is an efficient, inexpensive technique in which the whole apparatus is compact. It involves the generation of a strong electric field between a polymeric solution and a metallic collection plate (Fig 3.10). A drop (bead) of the polymeric solution is formed at the tip of the reservoir that contains the solution and this drop is held by its surface tension. At the stage when the voltage reaches a certain critical value, the electric charge overcomes the surface tension and a charged jet or stream of the polymeric solution is formed. While traveling in air towards the grounded electrode (collection plate), the jet gets stretched[77], its diameter reduces, the

solvent evaporates and a random arrangement of polymeric fibers is formed on the plate. The fiber diameter and pore size can be controlled by varying the process parameters such as the polymeric concentration, distance between the tip of the reservoir and the collection plate and electric field strength. The reinforcement material can be incorporated by dispersing it in the polymeric solution and co-electrospinning.

To date polyurethane, polycarbonate, polyacrylonitrile, PVA, and PLLA, etc have been electropun to produce nanofibers[78]. As long as the polymer can be electrospun to form fibers, the collector plate should have a surface that is smooth and defect free.

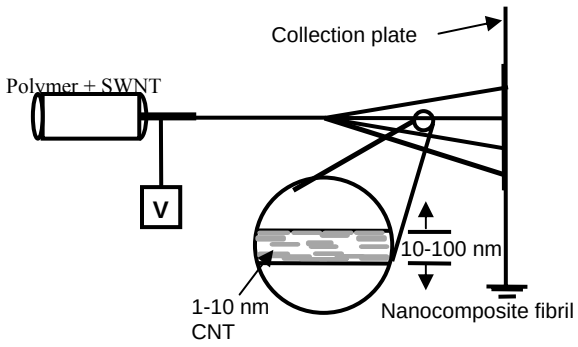

Figure 3.10. Schematic of the electrospinning set-up.

Electrospinning has been used to produce nanofibers reinforced with carbon nanotubes. A study by Ko et al utilized co-electrospinning as a method to align SWNT in the polymeric composite in order to form a planar, 3-D structure[48]. The purified SWNT were dispersed in polyacrylonitrile (PAN) solution and electrospun.The structure, composition and physical properties of this composite structure were characterized by Raman spectroscopy, TEM, AFM, and TGA. The AFM images of the composite fibril (fig 3.11) revealed that the composite had a rough surface compared to the smooth surface of the PAN fibrils. This was further collaborated with TEM images which confirmed the presence of SWNT along the fiber orientation. The composite showed a 15ºC increase in decomposition temperature compared to PAN. AFM tapping mode was used to evaluate the mechanical properties of the fibril and this showed a ductile mode of failure and doubling of the tensile modulus with respect to a pure PAN fibril.

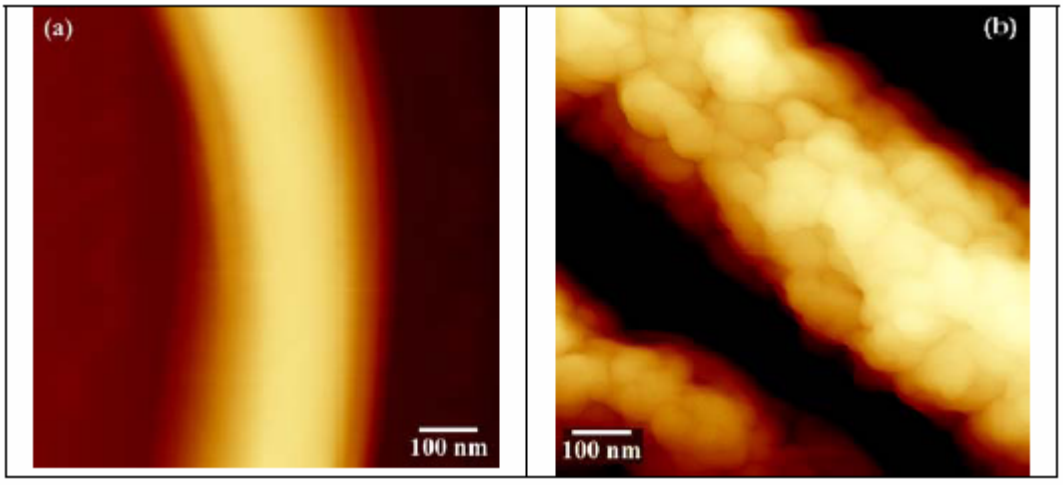

Figure 3.11. AFM images of (a) pure PAN fiber; (b) PAN/SWNT composite fibril.

A polymeric, fibrous scaffold reinforced with carbon nanotubes can provide the necessary surface for chondrocyte attachment and can thus be used for articular cartilage regeneration. Electrospinning fabricates a matrix characterized by high porosity and fibers on the nanometer scale. The advantage of a nanofibrous matrix is that it provides large surface area for cell attachment and the porosity allows for cell migration as well as transport of nutrients.

In this study, we have aimed at increasing the mechanical properties of a scaffold to be used for cartilage regeneration. To this end, we have electrospun a nanocomposite scaffold that is three dimensional, fibrillar and polymer-based reinforced with SWNT.

CHAPTER 4 : METHODOLOGY

All the concentration measurements were done in weight by weight (w/w). For a comparative study, four types of scaffolds were prepared containing, namely, PLLA (P), PLLA/ε-PL (PK), PLA/SWNT (PC) and PLLA/SWNT/ε-PL (PKC). In all solutions, the concentration of PLLA was kept constant at 2.5%. Purified single walled carbon nanotubes (SWNT) grown by the high pressure carbon monoxide deposition process (HiPCO) were supplied by Dr. Peter Willis of NASA-JPL. These SWNTs and dried for four hours at 130°C and then dispersed in Di-methyl formamide (DMF) to obtain a uniform dispersion. The polymer was dissolved in solvent choloform ($CHCl_3$) by simultaneous heating and stirring.

In fig.4.1, the step-wise procedure that was used to carry out this study has been outlined. After the four types of scaffolds were fabricated using the technique of electrospinning, they were individually characterized by scanning electron microscopy (ESEM), transmission electron microscopy (TEM), and Raman Spectroscopy. They were also subjected to tensile tests in order to determine their mechanical properties such as maximum stress, elastic modulus and elongation at break. A separate set of scaffolds were coated with collagen overnight and then seeded with human chondrocytes. They were then studied for a period of nine weeks at various time points and were characterized by ESEM and MTT (3,[4,5-dimethylthiazol-2-yl]-2,5-diphenyltetrazolium bromide) Assay.

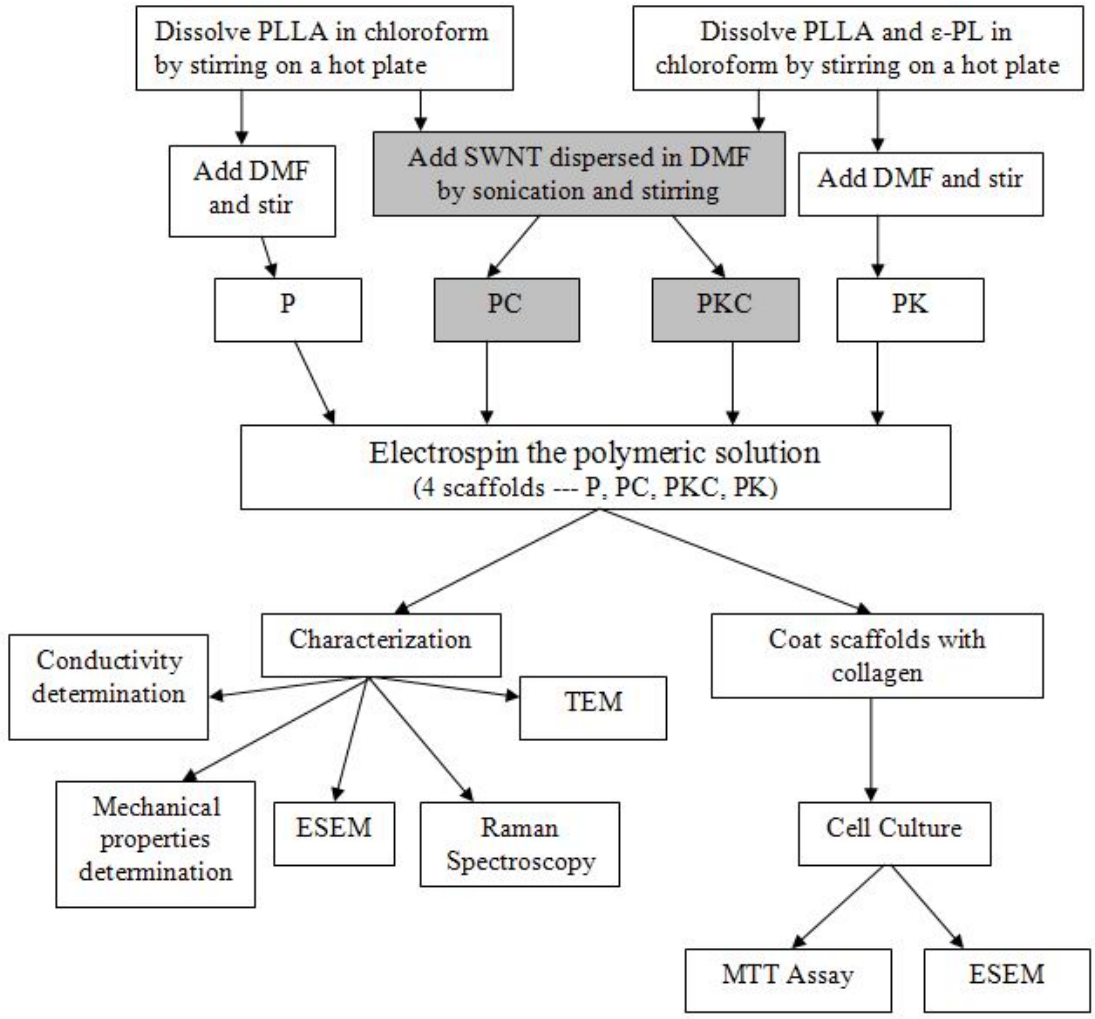

Figure 4.1 Flow chart depicting design of experiment

4.1 Spinning Dope Preparation

In all solutions, the concentration of PLLA was kept constant at 2.5%. In scaffolds PK and PKC, the concentration of ε-PL was one-fourth that of PLLA. In PC and PKC, the concentration of CNT was 1% of total dry weight (Table 1).

PLLA dissolves in chloroform. But, chloroform has a very rapid evaporation rate and tends to clog the pipette tip during the electrospinning process preventing further formation of matrix. To avoid complete evaporation of chloroform during electrospinning, di-methyl formamide was also used as solvent. So, the solvent system chosen to dissolve PLLA (MW 300,000) (Polyscience Inc.) was 5:1 chloroform (Fischer Scientific) and di-methyl formamide (DMF) (Fischer Scientific). For the scaffold PK, PLLA and ε-PL were dissolved simultaneously in the same above mentioned solvent.

Table 4.1. Composition of each fabricated scaffold

Components	Scaffolds			
	P	PK	PC	PKC
PLLA	2.5%	2.5%	2.5%	2.5%
Poly-ε-L-Lysine	0	0.6%	0	0.6%
SWNT	0	0	0.025%	0.025%

PLLA- Poly-lactic acid
SWNT- Single-walled carbon nanotubes
P- PLLA scaffolds
PK- PLLA and Poly-ε-L-Lysine scaffolds
PC- PLLA with SWNT scaffolds
PKC- PLLA with Poly-ε-L-Lysine and SWNT scaffolds

4.2 Dispersion of SWNT

Single-walled carbon nanotubes tend to form stabilized clusters (or bundles) in a solvent due to the presence of van der waals forces. These clusters evolve into ropes too. In order to avoid cluster formation, for the scaffolds PC and PKC, the required amount of purified SWNT was dispersed in DMF by alternating between sonication (Ultrasonic sonicator maintained at 60°C) and stirring on a magnetic stir plate for a period of four hours, to obtain an even distribution of SWNT in the solution. The polymer system was prepared separately by dissolving in chloroform and later being added to the mono-dispersed SWNT/DMF solution.

4.3 Electrospinning of Fiber Mat

Electrospinning is an efficient, inexpensive technique in which set-up is compact. It involves the generation of a strong electric field between a polymeric solution and a metallic collection plate (Fig.4.2). A drop (bead) of the polymeric solution is formed at the tip of the reservoir that contains the solution and this drop is held by its surface tension. At the stage when the voltage reaches a certain critical value, the electric charge overcomes the surface tension and a charged jet or stream of the polymeric solution is formed. While traveling in air towards the grounded electrode (collection plate), the jet gets stretched, its diameter reduces, the solvent evaporates and a random arrangement of polymeric fibers is formed on the plate. The fiber diameter and pore size can be controlled by varying the

process parameters such as the polymeric concentration, distance between the tip of the reservoir and the collection plate and electric field strength. The reinforcement material can be incorporated by dispersing it in the polymeric solution and co-electrospinning. A required thickness of the fiber mat can be fabricated taking into account the amount of fiber collected per hour. Electrospinning fabricates a light-weight matrix characterized by flexibility, high porosity and fibers on the nanometer scale. Thus, electrospinning permits tailoring of the properties of the scaffold to suit any requirement in terms of shape, mechanical properties, porosity, fiber diameter etc. The advantage of a nanofibrous matrix is that it provides large surface area for cell attachment and the porosity allows for cell migration as well as transport of nutrients.

Figure 4.2. Schematic of the electrospinning set-up

In this study, the polymer-solvent solution was placed in a pipette at a distance of 15cm (horizontally) from the collection plate and at an angle of 30° to the horizontal. A copper plate covered with aluminum foil was used as the collector plate. A copper wire placed into the solution in the pipette acted as the positive electrode. The electric field between the grounded collection plate (cathode) and the copper wire (anode) was constant at 1 V/cm.

4.4 In-vitro Cell Study

The four scaffolds (P, PK, PKC and PC) were used to study chondrocyte attachment and proliferation in them. The scaffolds were first coated with collagen using the method developed by Zheng[79] et al. The scaffolds were placed in a 4.5*M* HCl solution in glacial acetic acid and incubated for 30 min at 37°C. 0.1M sodium carbonate was added to neutralize the scaffolds and these were then stored in sterile water maintained at 4°C. Collagen stock solutions were diluted to a concentration of 200 mg/mL with 10 m*M* of MOPS [3-(*N*-Morpholino)propanesulfonic acid]. The pH was adjusted to 4.5 using 5 mg/mL of water-soluble carbodiimide [1-ethyl- 3-(3-bimethylaminopropyl) carbodiimide]. The scaffolds were left overnight at 4°C to allow the activated amino groups to react with the collagen. The scaffolds were then washed with 10 mM of HCl, followed by water in order to remove the unbound collagen.

The control sample of this study was the scaffold P. The nanofibrous scaffolds were sterilized by ultraviolet radiation (UV rays) and then washed successively with ethanol (70% concentration) and Dulbecco's modified eagle's medium (DMEM). Six samples of area 1cm^2 from each of the four types of scaffolds were then coated overnight with type II collagen. The scaffolds were then placed in individual tissue culture wells and seeded with 20,000 human chondrocytes (Cell Applications Inc) each along with cell media and placed in an incubator at a temperature of 37°C (Therma Forma HEPA Filter Series – Water jacketed CO_2 Incubator). The wells were periodically drained and fed with fresh media. Cell morphology and viability were studied using ESEM and MTT assay respectively.

CHAPTER 5: CHARACTERIZATION

Upon fabrication, the fiber mats were characterized by several techniques. Small portions of the mats were imaged under a scanning electron microscope to get topographical information about their fibrous structure. The fiber diameters were also measured at various locations and an average fiber diameter was calculated based on the average of 100 measurements. Raman spectroscopy was used in order to confirm the presence of single walled carbon nanotubes in the fibers of scaffolds PC and PKC. The presence of SWNT and their orientation along the fiber orientation was examined using transmission electron microscopy. The scaffolds were also subjected to mechanical tests to measure their mechanical properties. For the *in-vitro* study, the scaffolds seeded with human chondrocytes were imaged (after fixing), at various pre-decided time points, using SEM. The *in-vitro* study was carried out for a period of nine weeks and them the scaffolds were subjected to the MTT (3,[4,5-dimethylthiazol-2-yl]-2,5-diphenyltetrazolium bromide) assay to detect viability of cells on the scaffolds.

5.1 Physical and Mechanical Characterization of Scaffold

5.1.1 Field Emission Environmental Scanning Electron Microscopy (ESEM)

While conventional light microscopes use a series of glass lenses to bend light waves to view magnified images, scanning electron microscopy (SEM) creates magnified images by using electron beams. In SEM, as the samples are illuminated with electrons, they have to be made to be conductive so that they can

bounce off the electrons. A sample can easily be made conductive by coating it with a thin layer of gold in a gold sputtering machine. The samples are then placed into the SEM chamber and the air is pumped out of the chamber creating a vacuum. An electron gun positioned at the top of the set-up emits a beam of high energy electrons which travels down the column through a series of magnetic lenses designed to focus the beam to a very fine spot. The beam hits the sample producing secondary electrons and these backscattered electrons are collected by a secondary detector, converted to a voltage, and amplified. This amplified voltage is displayed on a cathode ray tube (CRT) and this display corresponds to the surface topography as well as morphology of the sample. The advantage of using SEM over conventional light microscopy is that SEM offers high resolution of images, thus even very closely spaced features can be studied.

While conventional SEM requires a high vacuum in the specimen chamber to prevent atmospheric interference with the electrons, ESEM can be operated even with poor vacuum (as much as 10 Torr of vapor pressure) in the specimen chamber. For this “environmental” aspect to be incorporated, the upper and lower portions of the vacuum column should be totally isolated from the specimen chamber. The imaging gas in this equipment is water vapor. When the electron beam (primary electrons) strikes the sample surface, secondary electrons are emitted from the surface of the sample and these secondary electrons collide with water molecules (present in the specimen chamber) and as a result, the water molecules emit secondary electrons of their own which makes the adjacent water

molecules also emit secondary electrons. This way, the water vapor acts as a cascade amplifier, amplifying the original signal from the sample. The amplified secondary electron signal is collected at a positively biased gaseous secondary electron detector (GSED). So a very good signal from the sample is obtained, and as the electron beam moves across the sample at a given point, the intensity of that signal is converted into a brighter or darker portion of the image.

The main advantage of ESEM over SEM is the fact that the material need not be made conductive by coating with gold or palladium and so the sample's original characteristics may be preserved for further testing. The sample can also be modified and imaged later as its original characteristics have not been altered by a conductive coating. Also, as the field-emission gun produces a brighter primary electron beam, its accelerating voltage may be lowered significantly, thus permitting imaging of even fragile samples.

A piece with dimensions of 1cmx1cm was cut out of each of the scaffolds, gold coated in a Denton Desk II Sputtering System (Fig 5.1), and examined in a Phillips XL-30 field emission environmental scanning electron microscope (Fig 5.2). The acceleration potential of the microscope was maintained at 15kV. In the case of the samples containing chondrocytes, prior to imaging, the cells were fixed by suspending the scaffolds separately in 2.5% glutaraldehyde for two hours at room temperature. They were then washed three times with distilled water for 10 minutes. Ethanol-phosphate buffered saline solutions of various concentrations

(25%, 50%, 75%, 90% and 100% of ethanol) were used to dehydrate the samples. The samples were further dehydrated with 1,1,2-Trichlorotrifluoro-ethane (Sigma-Aldrich). These dry cellular constructs were then coated with gold in a sputtering machine and observed under the microscope.

Figure 5.1. Denton desk II sputtering machine

Figure 5.2. Phillips XL-30 field emission environmental scanning electron microscope.

5.1.2 Transmission Electron Microscopy (TEM)

The internal structure of materials can be determined or viewed through transmission electron microscopy (TEM). Like SEM, TEM also utilizes an electronic beam for imaging purposes. The electron beam is passed through the very thin sample and the image forms on a fluorescent screen.

TEM images of the PC and PKC samples were taken on a JEOL.JEM 2010 F field emission microscope. The samples were cut to fit into the Lacey Carbon coated copper grids which had a diameter of 3mm. The accelerating potential through the entire imaging was maintained at 200 kV. The presence as well as their orientation of SWNT within the fibrous structures was observed at low magnification. The amorphous nature of the polymeric matrix was also observed.

5.1.3 Raman Spectroscopy

Raman spectroscopy is based on the Raman Effect and involves the measurement of the wavelength and intensity of inelastically scattered light from molecules. In the Raman Effect, the energies of the incident and scattered photons are different and this difference in energies of the molecular vibrations causes the wavelengths of the incident light to shift and scatter.

Each molecule has a “fingerprint” or Raman spectrum specific to itself. To detect the presence of SWNTs in the electrospun PC and PKC scaffolds, Raman

spectroscopy analysis was conducted. Samples from the above mentioned two scaffolds were cut into small pieces and observed in the Renishaw Raman microspectrometer RM1000 (Fig 5.3). The excitation wavelength was 780 nm and power density was 12 W/cm^2. The Raman spectra of SWNT has intense peaks near 180 cm^{-1} corresponding to the radial breathing mode (RBM) and another band of peaks between 1500-1600 cm^{-1} corresponding to the frequency of the graphite mode[80]. The intense peaks in the 1500-1600 cm^{-1} range correspond to the G band while the single peak in the 1200-1300 cm^{-1} range corresponds to the D band. The D mode is the disordered carbon mode attributed to the presence of amorphous carbon in samples[81]. The G band is associated with the tangential displacement of the carbon-carbon (C-C) bond stretching motion of the nanotubes. The RBM frequency believed to be inversely proportional to the diameter of the tube and independent of the chiral angle. The frequencies and the number of the Raman peaks between 1500-1600 cm^{-1} depend on the diameter as well as chiral angle of the nanotube. RBM corresponds to the A1g or A1 radial band, the stretching mode corresponds to the tangential band (E1g or E2g symmetry)[82] meaning that the carbon atoms undergo a radially oriented displacement perpendicular to the nanotube axis.

Figure 5.3. Raman micro spectrometer

5.1.4 Mechanical Property Determination

The modulus of all four scaffolds (P, PK, PC, PKC) was measured using the Kawabata KES-G1 Microtensile Tester. The samples to be tested were 5mm x 40mm strips and four such samples were taken from each scaffold. The weight of each individual sample was recorded. The sample was mounted onto a rectangular paper frame (fig 5.4). The gauge length for all samples was 50 mm and the strain rate (extension) was maintained at 2mm/second, load was applied from the machine and the deformation was recorded. Stress-strain curve was obtained from load-deformation data and the corresponding equation relating them. The modulus was taken to be the initial slope of the stress-strain curve.

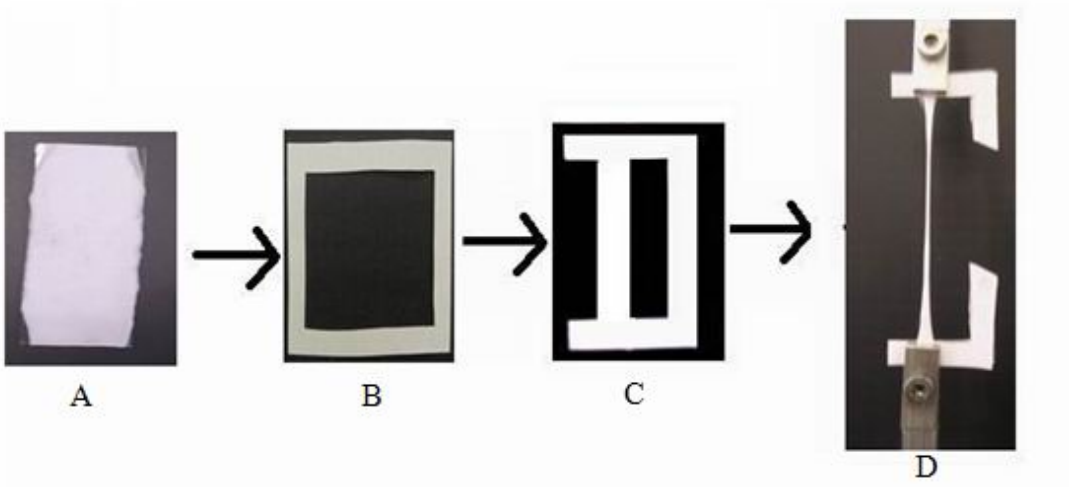

Figure 5.4. Mechanical test sample. A. Sample B. Rectangular paper frame C. Sample mounted on paper frame D. Sample undergoing tensile test.

5.1.5. Conductivity Measurement

The conductivity of the four scaffolds was determined using the Four-Probe Device (ALESSI CPS-06 Contact Probe). The concept of this test is to measure the conductivity (σ) of the material by first determining the resistance of the sample using Ohm's law and then calculating the resistivity (ρ). Ohm's law which states that the voltage (V) is proportional to the current (I) flowing through the circuit allows the resistance (R) to be determined (V=IR). Resistivity (ρ) of a material is the resistance provided by a uniform wire of length 1m and area of cross-section of 1 m^2 (ρ=RA/L). Conductivity is the inverse of resistivity. The device has four probes placed side-by-side in parallel, and with a precise separation between them. All four probes are connected to individual copper

terminal blocks. The current is passed through the outer two probes and the voltage drop is measured across the inner two probes (Fig. 5.5).

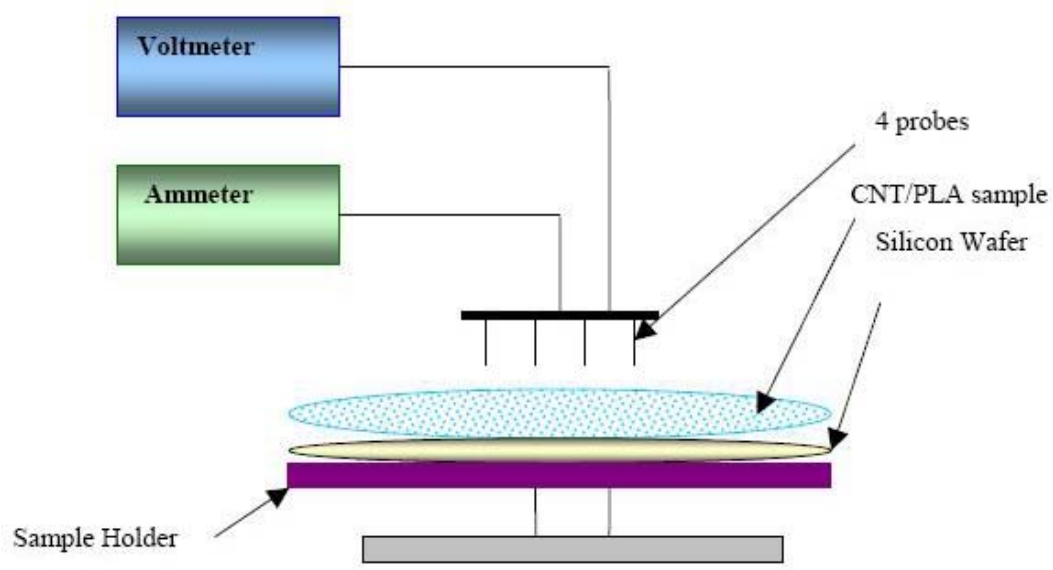

Figure 5.5. Four probe conductivity test showing the 4 probes.

For this test, the PC and PKC samples were electrospun directly onto a silicon wafer (Fig. 5.6). This wafer-sample combination can be viewed as two resistors in parallel when tested in the four-probe device (Fig. 5.7). Both the resistors, the silicon wafer (R_1) and the sample (R_2) are circular with the same diameter (10 cm) and therefore, the same area of cross-section (7.86×10^{-3} cm^2). The slope of the voltage-current data acquired for varying the current through the probes, gives the resistance of the sample. The resistance R_1 is measured by testing the silicon

wafer alone. The resistance R_2 can be calculated using the equation for two resistors in parallel ($1/R=1/R_1+1/R_2$). Once the resistance was found out, the resistivity and conductivity of the material were also found using the equations mentioned above in this section.

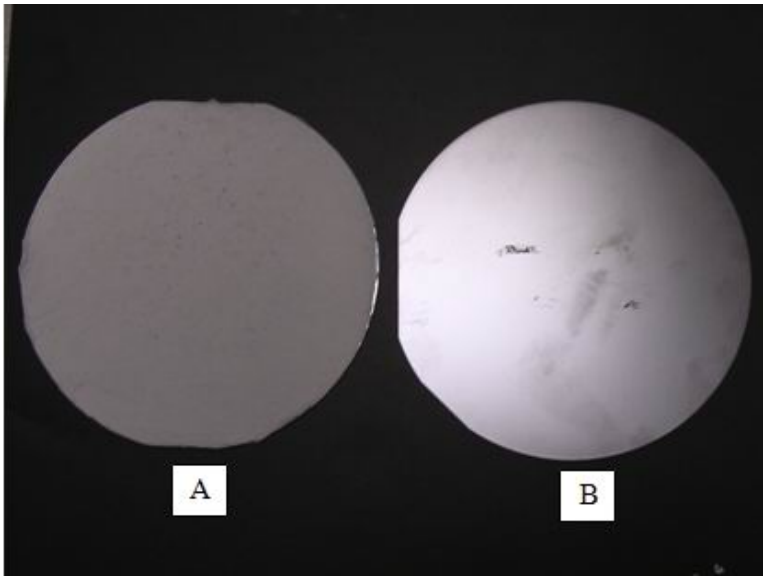

Fig 5.6. Conductivity test sample. A. Sample electrospun on the silicon wafer. B. Silicon wafer

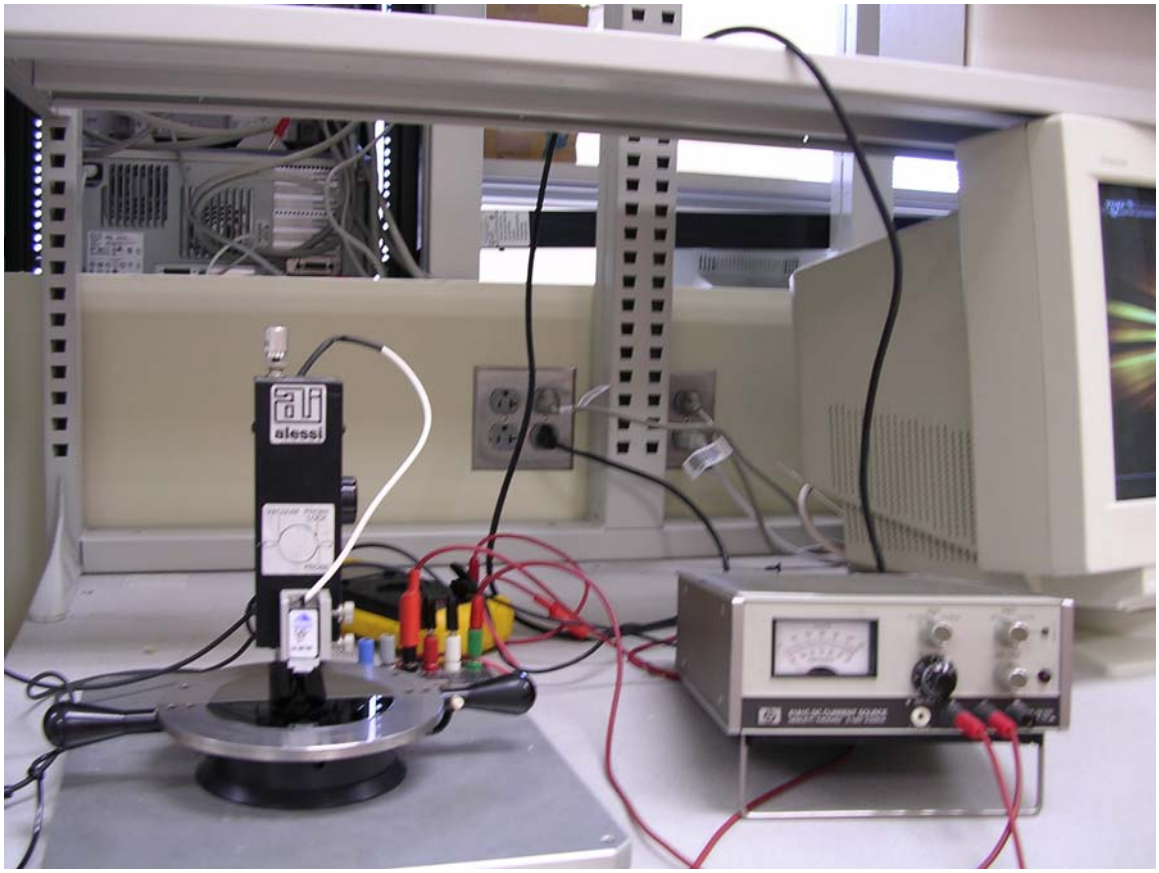

Figure 5.7. Four-probe device.

5.2 Characterization of Cell-Matrix Interactions

5.2.1 Field Emission Scanning Electron Microscopy (ESEM)

ESEM (Fig 5.2) was used to study the attachment and differentiation of human chondrocytes to the polymeric scaffolds. In order to image biological samples, the sample must be dried prior to the imaging to prevent shriveling and folding. In this study, at each time point, the cells were fixed by suspending the four, 1cm² scaffolds separately in 2.5% glutaraldehyde for two hours at room temperature.

They were washed three times with distilled water for 10 minutes. Ethanol-phosphate buffered saline solutions of various concentrations (25%, 50%, 75%, 90% and 100% of ethanol) were used to dehydrate the samples. The samples were further dehydrated with Freon (1,1,2-Trichlorotrifluoro-ethane) (Sigma-Aldrich) and placed under the hood overnight. These dry cellular constructs were then coated with gold in a sputtering machine and observed under the SEM.

5.2.2 MTT Assay

MTT assay was performed at the end of nine weeks to quantify the viable chondrocytes seeded on the four scaffolds. Mitochondria of viable cells cleave the pale yellow MTT and yield dark blue or purple formazan products. 2.5mg/ml MTT(Sigma Aldrich, Cat # 2128) was dissolved in phosphate buffer saline (PBS) and 200µL of this stock solution was added to each of the four wells containing the scaffold. The wells plate was then incubated for five hours at 37^{o}C, after which, the media was drained from the wells. In order to solubilise the cell wall, the scaffolds were taken out of the wells and put into individual eppendorfs which were fed with 0.1 ml of a 12M isopropanol-hydrochloric acid (HCl) solution and vortexed (Fischer Vortex Genie, Cat # 12-812). The four liquid products obtained as a result, were placed in the spectro-photometer (Spectronic Unicam, Genesys 8) (Fig.5.8) wells along with a solution of isopropanol and hydrochloric acid (HCl) used as blank. The absorbance of MTT on each sample was measured at 550nm. A higher absorbance implies more number of viable cells.

Figure 5.8. Spectro-photometer to measure absorbance.

CHAPTER 6: RESULTS AND DISCUSSION

6.1 Results from Physical and Mechanical Characterization of Scaffold

6.1.1 Morphology of the Scaffold

ESEM images were obtained for the four scaffolds P, PC, PK and PKC in order to view the fibrous nature of the scaffold as well as the morphology of the fibers. From these images, the fiber diameters were calculated taking an average of 100 measurements per image. The following figures (fig 6.1, 6.3, 6.5, 6.7) are the ESEM images for the four scaffolds.

Continuous fibers were obtained using a polymer concentration of 2.5% and electrospinning at a distance of 15cm under an electric field strength of 1V/cm. Fig. 6.1, 6.3, 6.5 and 6.7 show the absence of beads and the smooth surface morphology of the fibers obtained in the four scaffolds. As can be seen, the matrix is porous and has a random arrangement of fibers. This random arrangement of fibers mimics the morphology of the extracellular matrix of the articular cartilage.

The fiber diameter distribution plots for all four scaffold have been listed(Fig. 6.2, 6.4, 6.6, 6.8). They have also been fitted with a normalized curve aimed to show a trend (if any). The normalized curves show that the fiber diameter distribution is like a Gaussian curve.

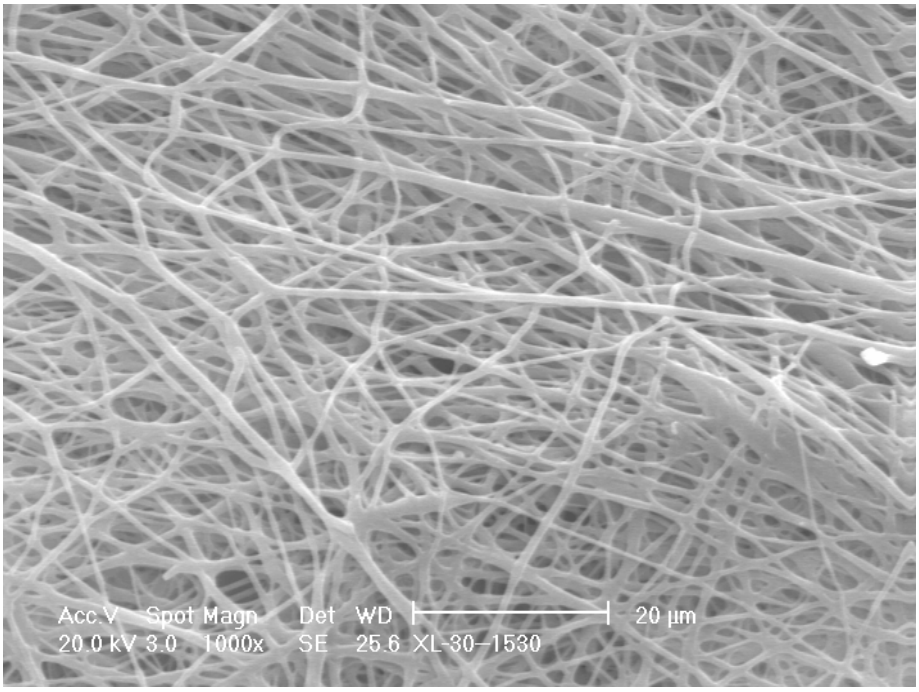

Figure 6.1. ESEM image of scaffold P.

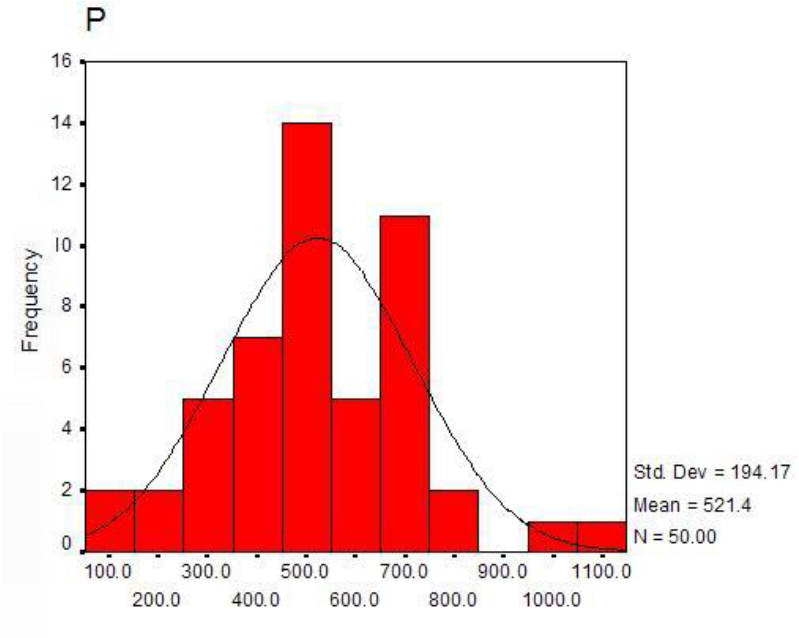

Figure 6.2. Fiber diameter distribution plot for scaffold P.

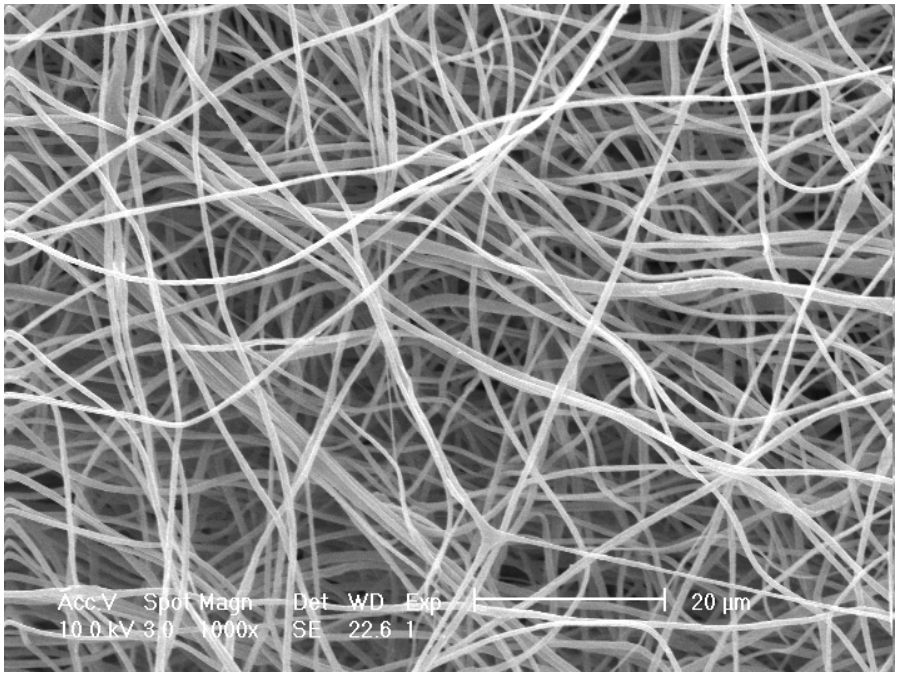

Figure 6.3. ESEM image of scaffold PC.

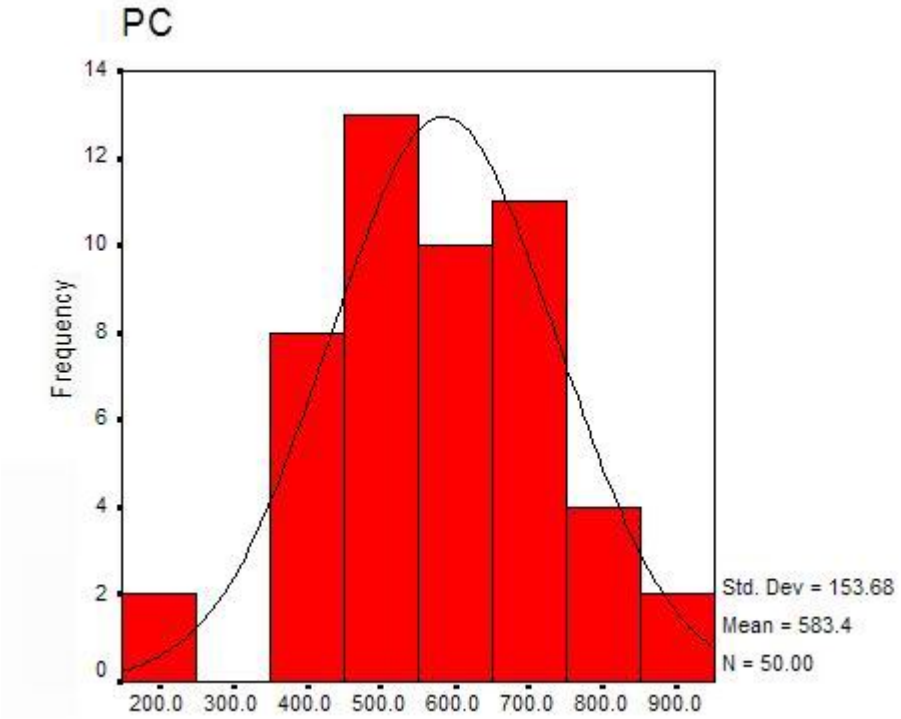

Figure 6.4. Fiber diameter distribution plot for scaffold PC.

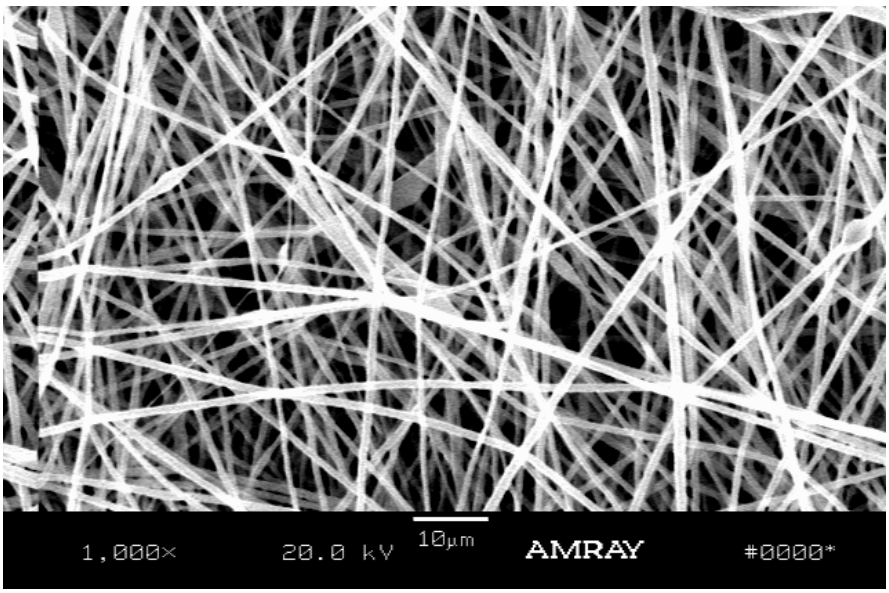

Figure 6.5. ESEM image of scaffold PK.

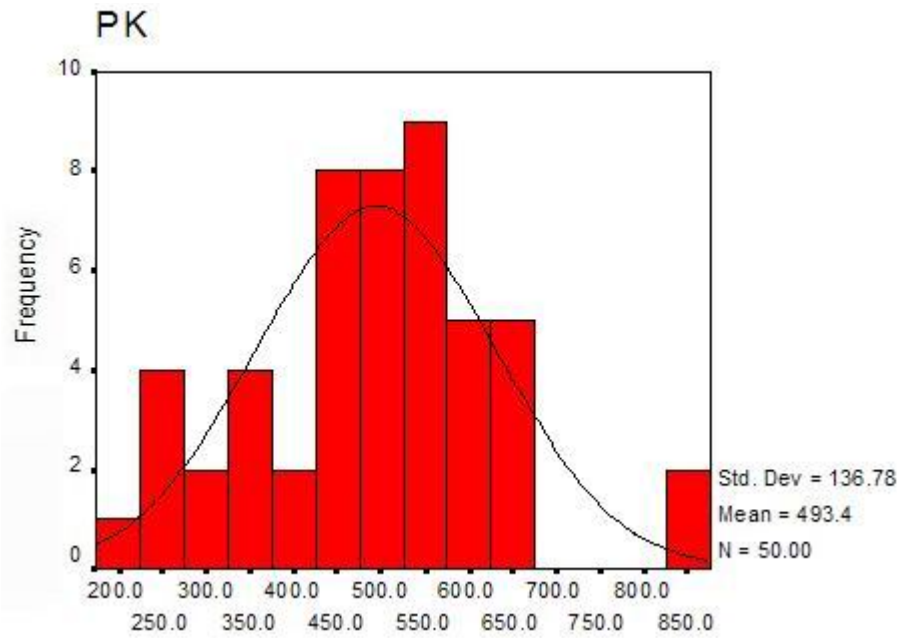

Figure 6.6. Fiber diameter distribution plot for scaffold PK.

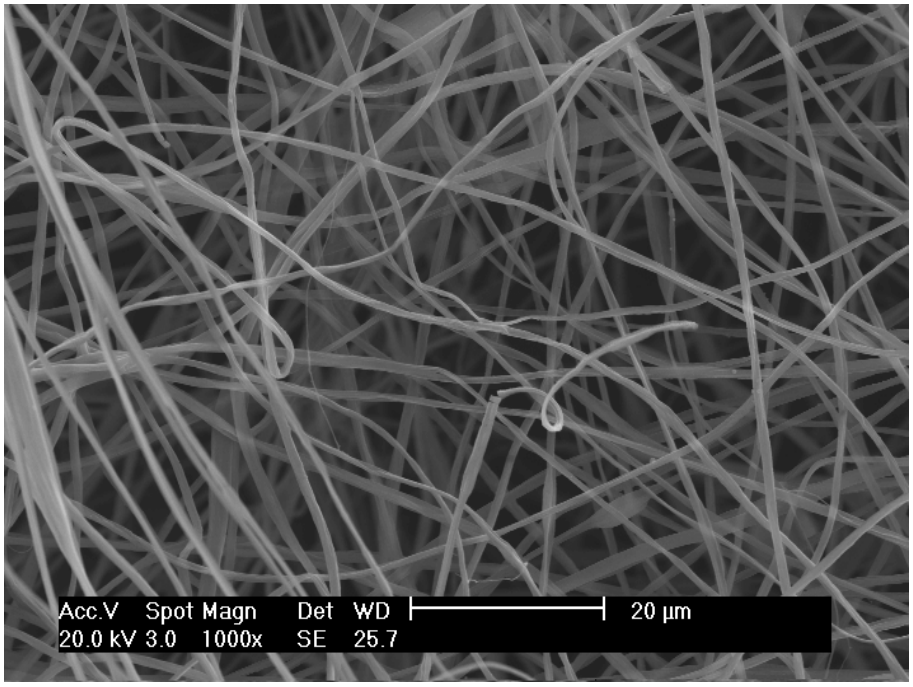

Figure 6.7. ESEM image of scaffold PKC.

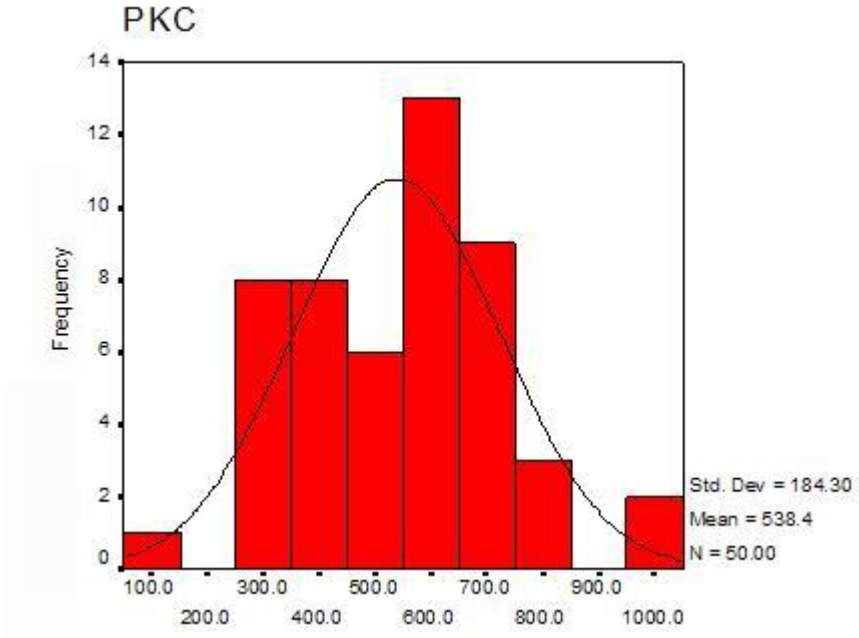

Figure 6.8. Fiber diameter distribution plot for scaffold PKC.

As can be seen in the summary of the ESEM images as well as the fiber diameter distribution plot for all four scaffolds (Fig.6.9), the fiber diameters range from as low as 150 nm to as high as 1 μm with average diameters in the range of 500 nm (with standard deviation of approximately 160 nm). All fiber distribution plots display a Gaussian distribution.

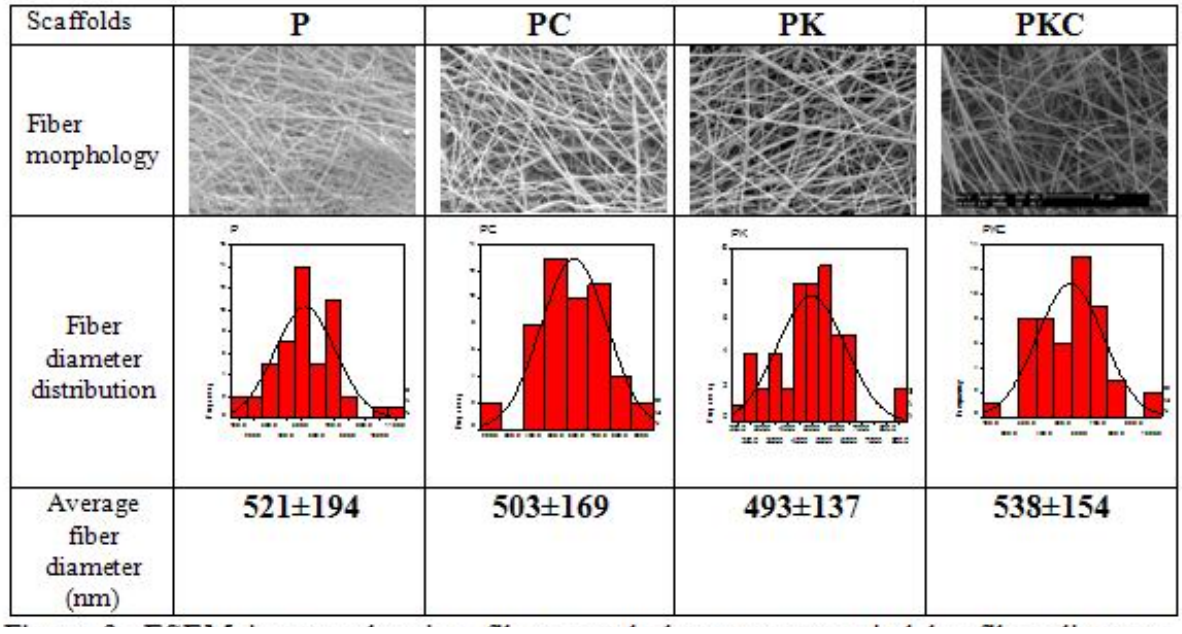

Figure 6.9. Summary of ESEM images, fiber distribution plots and average fiber diameters for scaffolds P, PC, PK and PKC.

6.1.2. Morphology of the Fiber

TEM images are expected the show the amorphous or crystalline nature of the fiber. In scaffolds containing SWNT, these images can show the orientation of the

nanotubes in the fiber. Below is a TEM image of a polymeric fibril containing no SWNT (fig 6.10). As can be seen, the fibers appear to have a rough and uneven morphology which is typical to an amorphous material displaying little crystallinity.

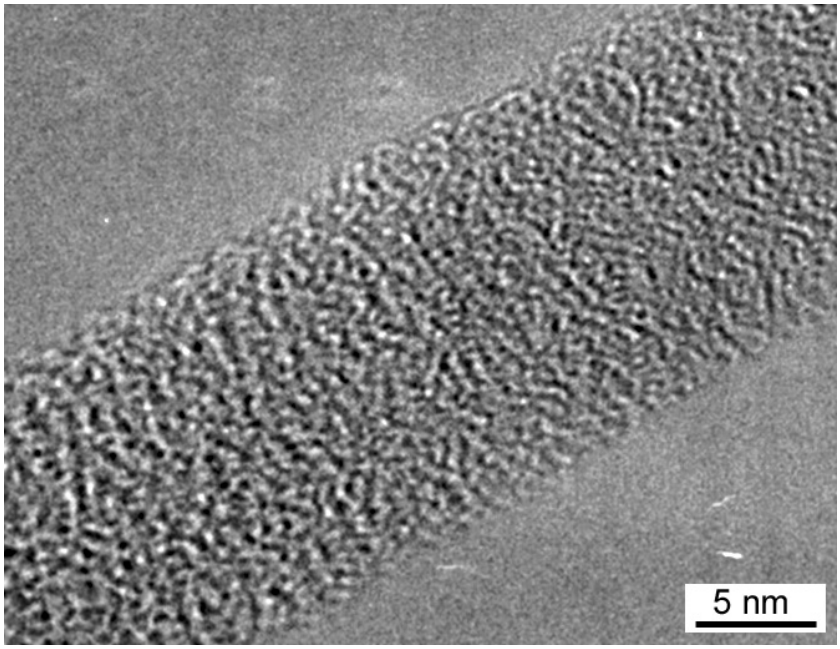

Figure 6.10. TEM image of a polymeric fibril.

TEM of a PC scaffold showed SWNTs aligned along the fiber orientation (Fig. 6.11) as well as protruding out of the fiber (Fig. 6.12, 6.13). Fig.6.13 shows two separate polymeric fibrils with a single SWNT protruding from each of their surfaces. The two SWNTs appear to be connected to each other and by this

means, the two polymeric fibrils have been held together. The fibers showed an element of crystallinity (attributed to the SWNT) but below the SWNTs, the amorphous morphology of the polymeric fiber itself was also seen. Bundles of SWNT were observed within the polymer fibers (Figure 6.11). The bundles were approximately 10 nm thick, implying that there were between five and ten nanotubes in the bundle, as the nanotubes are about 1-2 nm in diameter. There were several bundles lying parallel to each other. The bundles were of varying shapes and sizes and this variation could be attributed to the dispersion mechanism and also to the entanglement of the bundles.

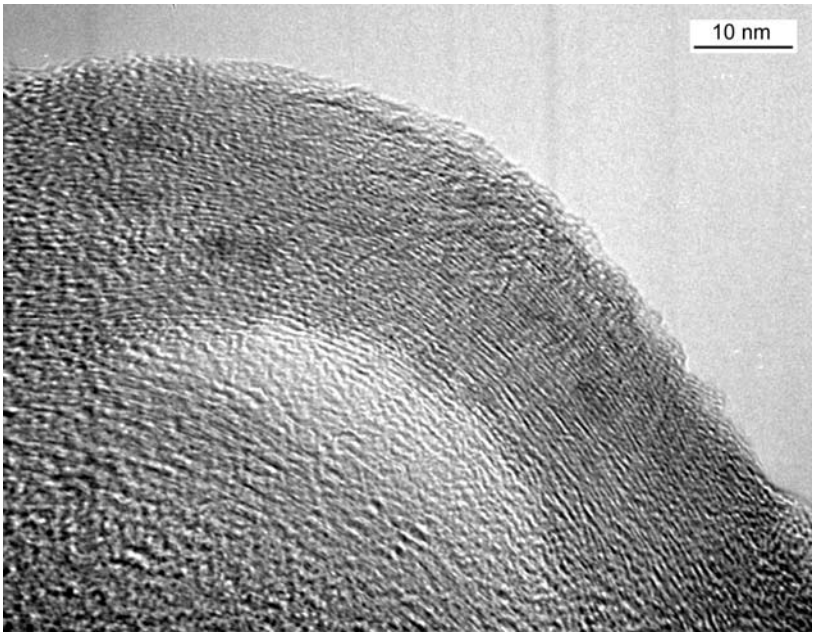

Figure 6.11. TEM image of SWNT aligned along the PC fiber.

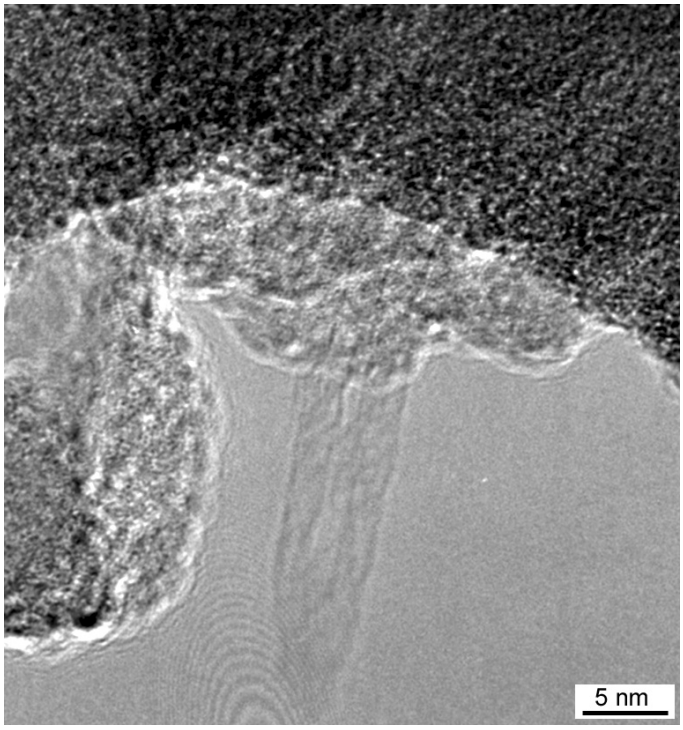

Figure 6.12. TEM image of SWNT protruding from the PC fiber.

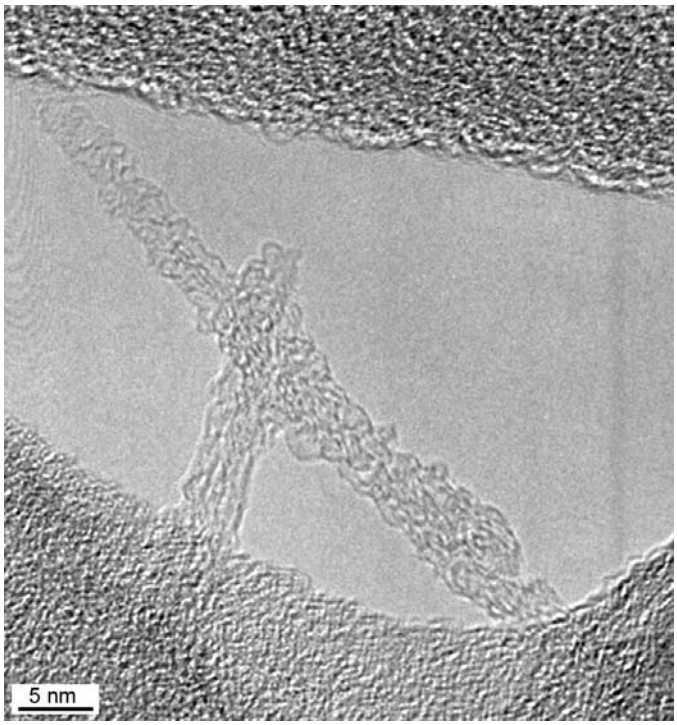

Figure 6.13. TEM image of SWNT protruding from adjacent PC fibers.

In the PKC fiber, the SWNT were aligned along the fiber orientation (Fig. 6.14), but there was no evidence of nanotubes protruding from the surface of the fiber.

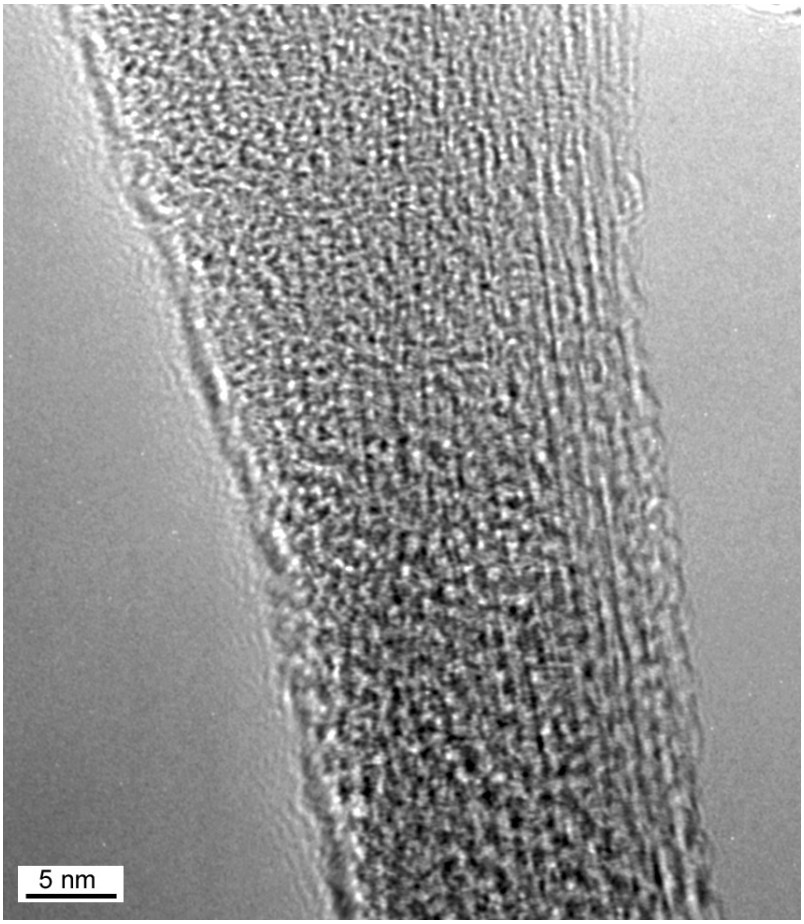

Figure 6.14. TEM image of SWNT aligned along PKC fiber.

Therefore, from the TEM images obtained, it is obvious that the SWNT are incorporated within and oriented along the fibers in the scaffolds PC and PKC and they also contribute crystallinity to the fibrous , polymeric matrix.

6.1.3 Raman Spectroscopy of the Scaffold

Raman spectroscopy was used as a tool to study the inclusion of SWNTs within the fibers. Raman spectrums were obtained for fibers in the scaffolds P, PK, PC and PKC and were compared with the spectra obtained for purified SWNTs. The spectra of the scaffolds containing SWNT (scaffolds PC and PKC) were similar to that of the SWNTs. They showed very sharp peaks of Raman active mode near 1590 cm^{-1} which is believed to be associated with the G band corresponding to the tangential displacement of the carbon-carbon (C-C) bond stretching motion of graphite in the nanotube walls (Fig.6.15). There is also a characteristic D band at 1293 cm^{-1}. Several intense peaks or SWNTs, the radial breathing mode (RBM) are seen near 210 cm^{-1}. These peaks are evidence of the successful inclusion of SWNT in the polymeric fibrils of the PC and PKC scaffolds. The fibrils of scaffolds P and PK showed no dominating peak for either graphite or SWNTs (which was expected). Intensity of spectra indicates the amount of nanotubes and as the peaks are quite intense, it implies that there are a large number of nanotubes within each fiber. Presence of multiple RBM peaks indicates wide range of tube diameter distribution in the polymeric fiber.

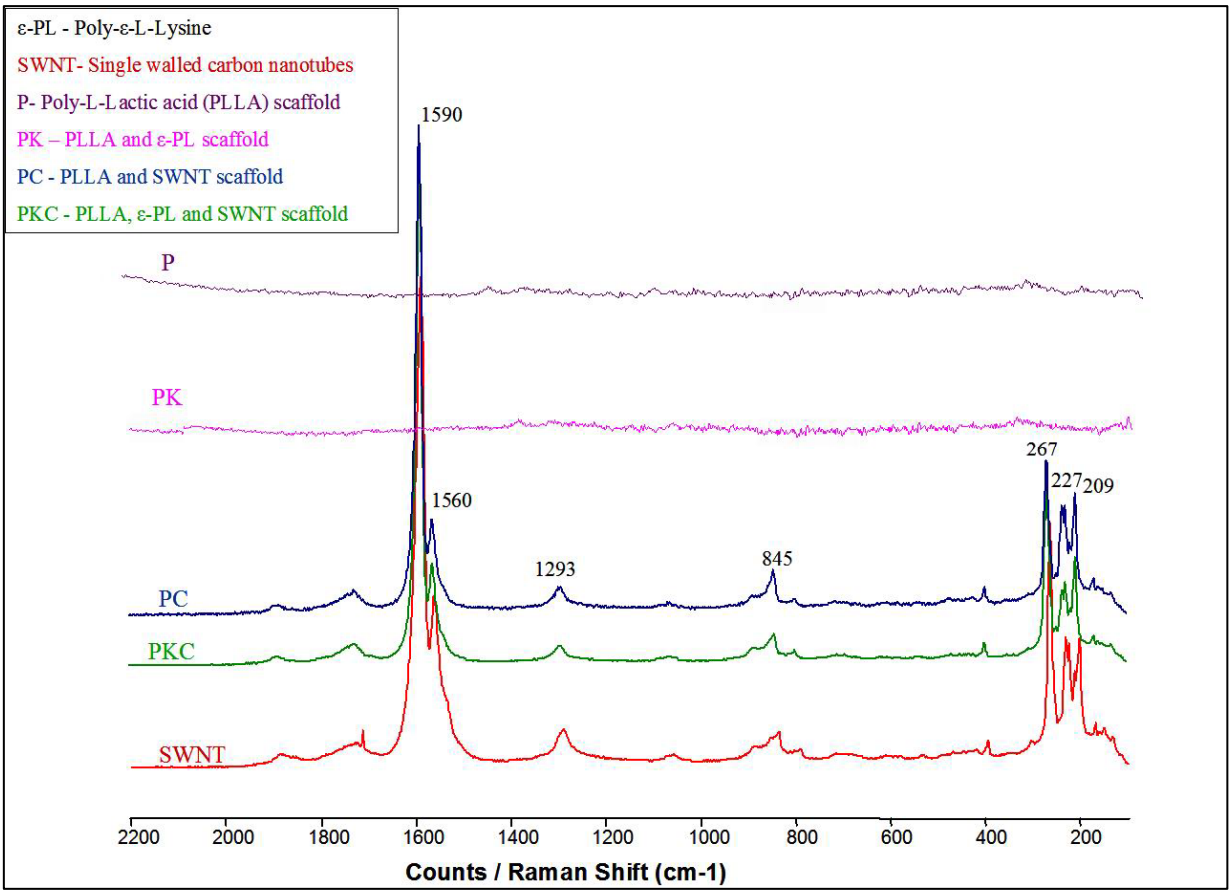

Figure 6.15. Raman Spectroscopy of SWNTs and scaffolds P, PK, PC and PKC.

The diameter of the carbon nanotubes can be calculated using the peaks in the RBM[83]. The frequency (ω_R) of the RBM is inversely proportional to the nanotube diameter (d)

$$\omega_R \sim 224\ cm^{-1}(nm)/d \qquad (1)$$

where d is in nanometer

The peaks in the RBM were at 267, 227 and 209 cm^{-1} and the average nanotube diameter was calculated using all three peaks and found to be 0.97±0.12 nm.

6.1.4. Mechanical Properties of the Scaffold

Three samples from each type of scaffold were tested to determine their mechanical properties such as modulus and tensile strength. The stress-strain plots for the four scaffolds are shown below (Fig 6.16, 6.18, 6.19, 6.20). As can be seen from the stress-strain plots, the curves are all linear up to the breaking point. From these plots, we can determine the ultimate stress, the modulus (initial slope of the curve) and toughness of fiber (area under the curve). The numerical values for the maximum stress, the modulus, elongation at break as well as toughness for the three samples have been shown below (table 6.1, 6.2, 6.3, 6.4).

The three samples tested for scaffold P, were labeled P1, P2 and P3. The stress-strain plot for this scaffold showed a non-linear curve. An ESEM image of the fractured surface has been shown below (fig 6.17) where it can be clearly seen that during the stretching process, the fibers unravel, get oriented parallel to themselves (aligned) and eventually break.

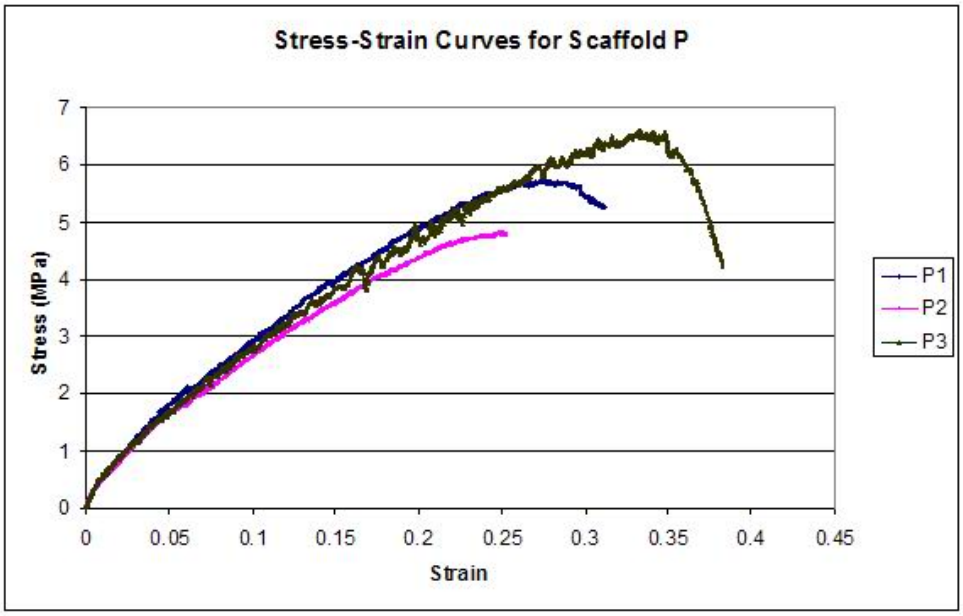

Figure 6.16. Stress-strain curves for the three samples of scaffold P.

Table 6.1. Mechanical property values for scaffold P.

Sample	Maximum Stress (MPa)	Modulus (MPa)	Elongation at break (%)	Toughness (MPa)
P1	5.74	44.38	28	0.978
P2	4.82	49.63	25	0.728
P3	6.63	72.92	33	1.328
Average	5.73±0.91	55.64±15.19	28.67±4.04	1.01±0.3

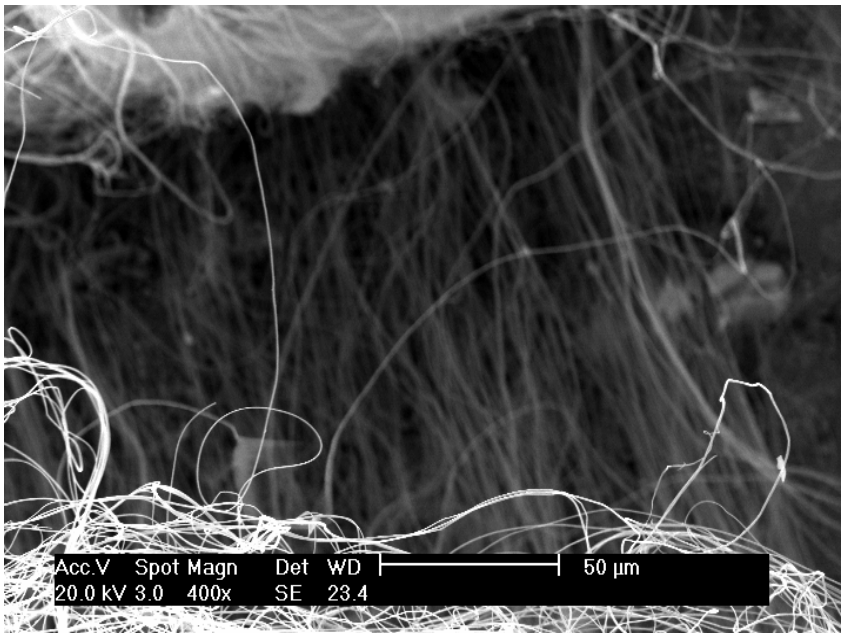

Figure 6.17. Fractured surface of scaffold P showing the alignment of fibers.

The three samples tested for scaffold PK, were labeled PK1, PK2 and PK3. This scaffold PK appears to be having more elongation than the P scaffold and also seems to withstand a higher stress. Its modulus however is slightly lower but is not significantly different (table 6.2). The stress-strain curve of this scaffold displays a non- linear plot upto the breaking point (6.18).

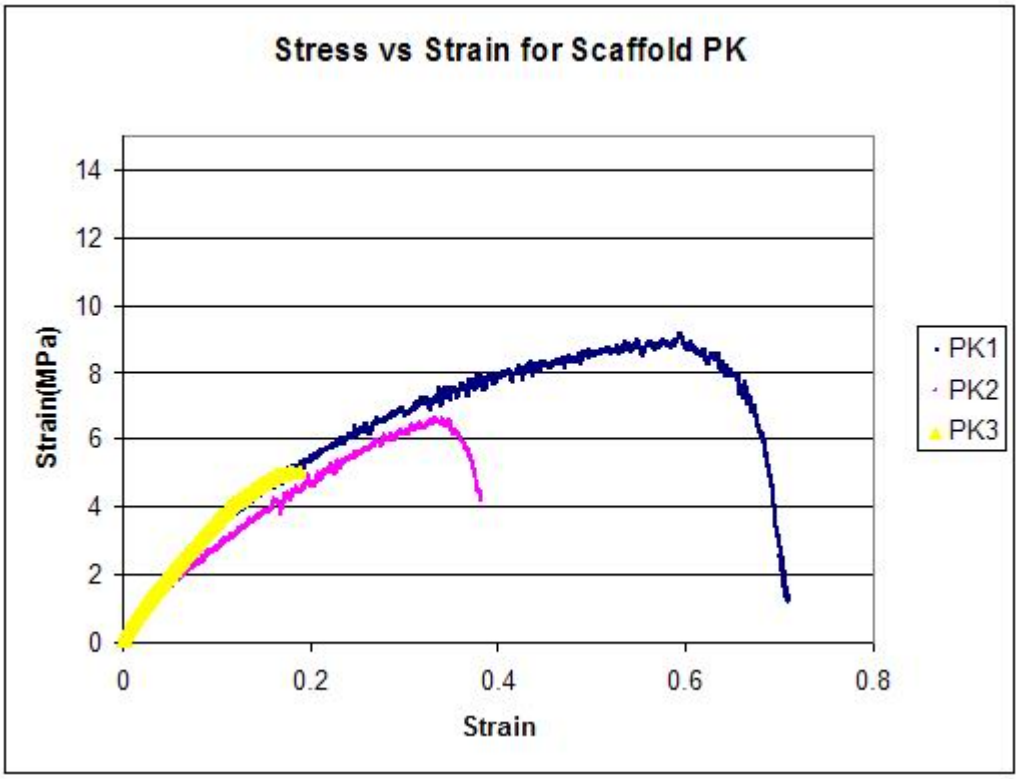

Figure 6.18. Stress-strain curves for the three samples of scaffold PK.

Table 6.2. Mechanical property values for scaffold PK.

Sample	Maximum Stress (MPa)	Modulus (MPa)	Elongation at break (%)	Toughness (MPa)
PK1	9.17	44.45	59	3.49
PK2	6.70	71.96	32	1.27
PK3	5.06	43.69	19	0.63
Average	6.98±2.07	53.37±16.11	36.67±20.4	1.8±1.5

The three samples tested for scaffold PC, were labeled PC1, PC2 and PC3. This scaffold PC appears to be less elastic (meaning, more brittle) than the P scaffold but it can withstand a higher stress. Its modulus however is much higher (almost 3

times) than scaffold P (Table 6.3), implying that incorporation of SWNTs has improved the mechanical properties of the polymeric scaffold. The toughness has also increased over the P scaffold. The stress-strain curve for this scaffold shows two distinct regions with a very high initial modulus (slope) and then a constant lower slope (fig 6.19).

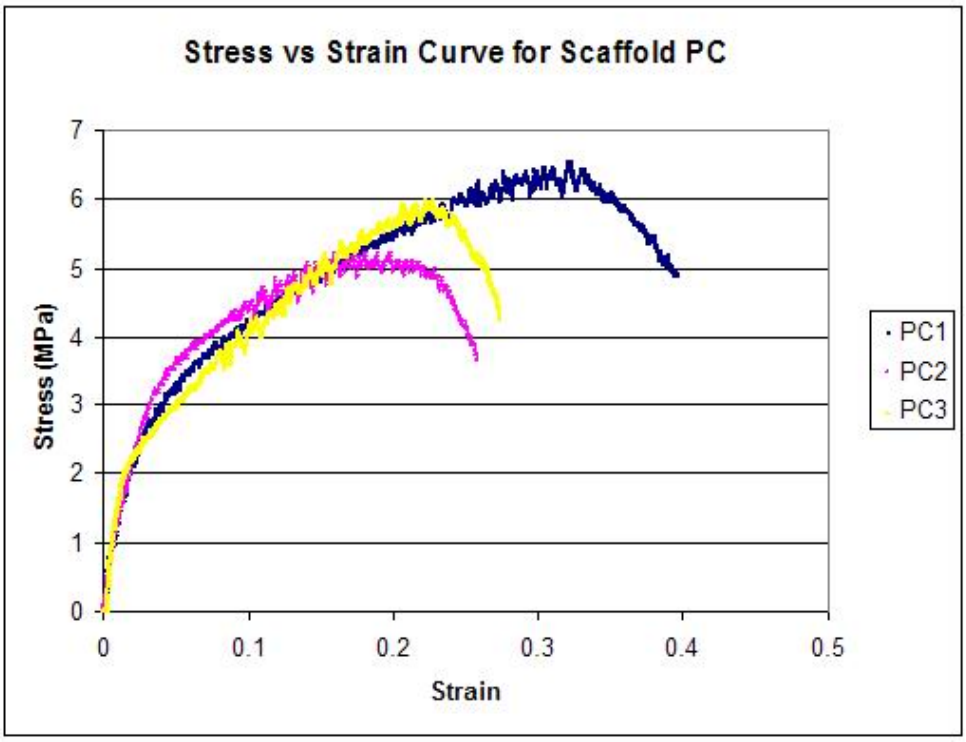

Figure 6.19. Stress-strain curves for the three samples of scaffold PC.

Table 6.3. Mechanical property values for scaffold PC.

Sample	Maximum Stress (MPa)	Modulus (MPa)	Elongation at break (%)	Toughness (MPa)
PC1	6.52	170.05	30	0.946
PC2	5.2	137.57	18	0.825
PC3	5.98	156.70	21	1.45
Average	5.9±0.66	154.77±16.32	23±6.24	1.07±0.33

The three samples tested for scaffold PKC, were labeled PKC1, PKC2 and PKC3. This scaffold PKC appears to be less extensible than the PK scaffold and withstands a higher stress. Its modulus is almost 2.5 times that of scaffold PK, but is a little lower than that of scaffold PC (Table 6.4). It is however, much tougher than both PK and P. The stress-strain curve for this scaffold also shows an initial high modulus region followed by a lower constant modulus (fig 6.20).

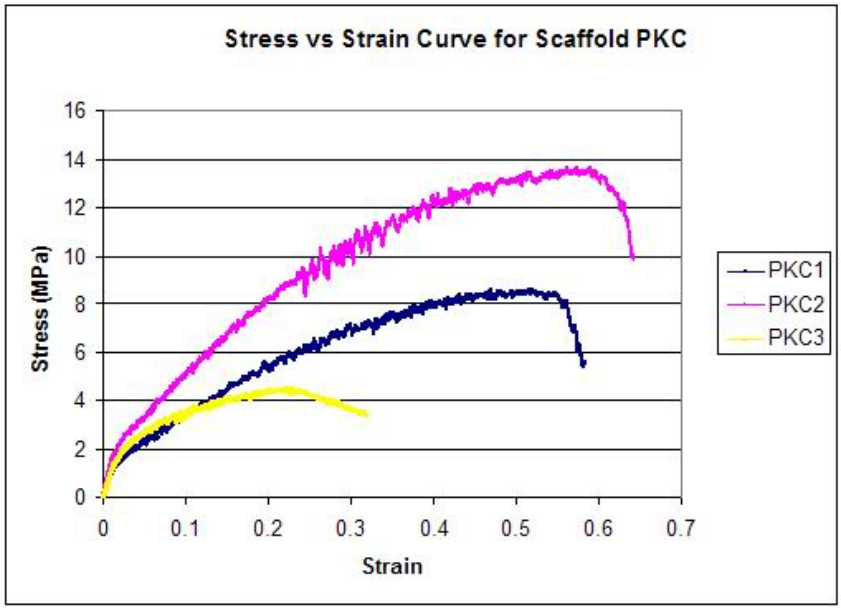

Figure 6.20. Stress-strain curves for the three samples of scaffold PKC.

Table 6.4. Mechanical property values for scaffold PKC.

Sample	Maximum Stress (MPa)	Modulus (MPa)	Elongation at break (%)	Toughness (MPa)
PKC1	8.61	111.95	47	3.25
PKC2	13.64	144.07	57	5.51
PKC3	4.55	116.05	22	0.75
Average	8.93±4.55	124.03±17.48	42±18.03	3.17±2.38

The tensile tests have revealed that the scaffolds containing SWNTs were able to withstand a higher stress than the corresponding unreinforced scaffolds. This can be explained taking into account the TEM images which have clearly shown that the SWNT are aligned within and along the fiber orientation, thereby improving the mechanical properties. The inter-connection of the SWNTs in scaffold PC has attributed to the high modulus of that scaffold. The improvement in maximum stress and modulus of scaffold PKC makes it a much more suitable scaffold to be used in vivo for cartilage repair as it is likely to perform better than the other three scaffolds in terms of dealing with the stresses at the joint.

6.1.5. Electrical Conductivity of the Scaffold

The four probe test was carried out to determine the electrical conductivity of the four scaffolds. The data collected during the four probe conductivity test has been listed in Appendix A (Table 1, 2, 3, 4, 5) and was obtained by gradually increasing the flow of current from zero to 2.1 mA in steps of 0.1 mA.

The current versus voltage graphs for each of the four scaffolds P (fig 6.21), PK (fig 6.22), PC (fig 6.23) and PKC (fig 6.24) has been listed below along with the numerical values for resistance of the scaffold (calculated using Ohm's Law), resistivity and conductivity.

Resistance of scaffold P	30211.87 Ω
Resistivity of scaffold P	1.78×10^{7} Ω-cm
Conductivity of scaffold P	5.6×10^{-8} $\Omega^{-1}cm^{-1}$

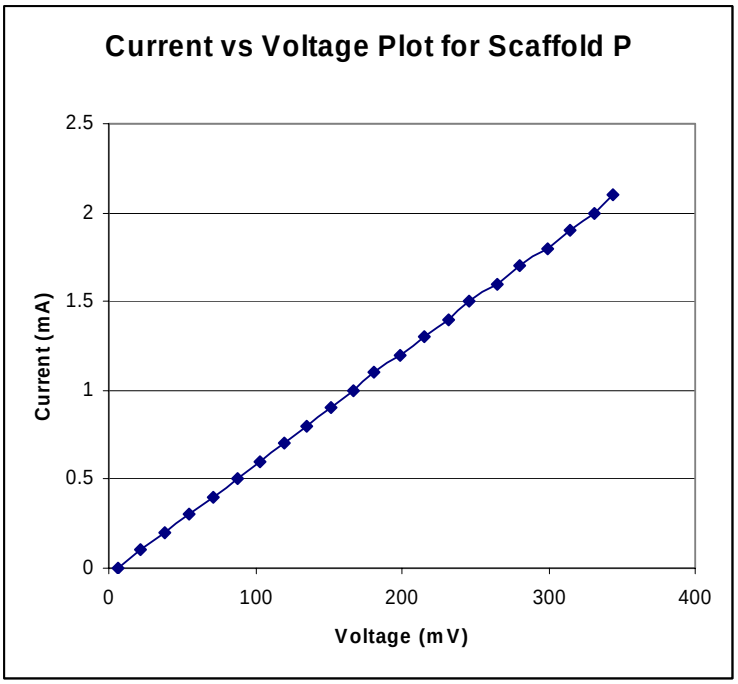

Figure 6.21. Current versus voltage plot for scaffold P.

Resistance of scaffold PK	23751.68 Ω
Resistivity of scaffold PK	1.4×10^{7} Ω-cm
Conductivity of scaffold PK	$7.13 \times 10^{-8} \Omega^{-1} cm^{-1}$

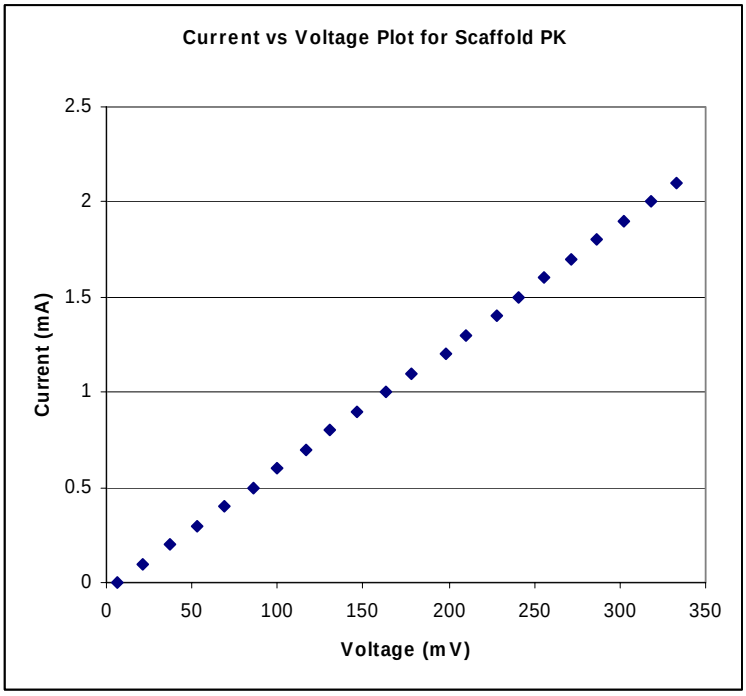

Figure 6.22. Current versus voltage plot for scaffold PK.

Resistance of scaffold PC	2.49Ω
Resistivity of scaffold PC	1495.45 Ω-cm
Conductivity of scaffold PC	$6.69 \times 10^{-4}\ \Omega^{-1} cm^{-1}$

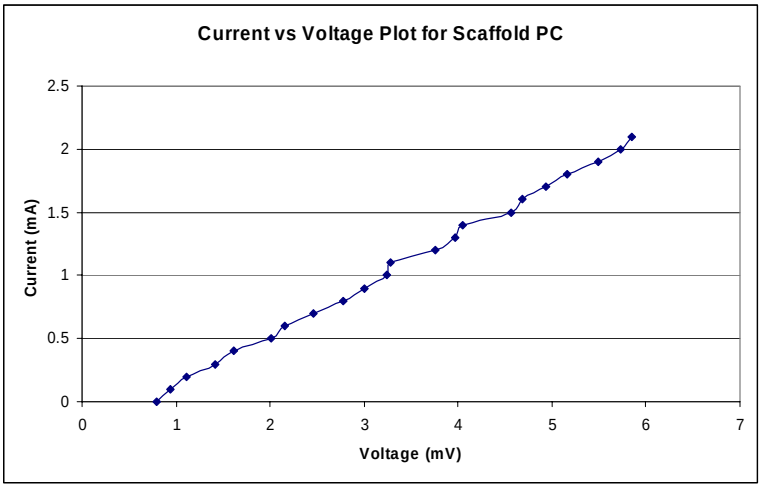

Figure 6.23. Current versus voltage plot for scaffold PC.

Resistance of scaffold PKC	2.83 Ω
Resistivity of scaffold PKC	1671.64 Ω-cm
Conductivity of scaffold PKC	$5.98 \times 10^{-4}\ \Omega^{-1}cm^{-1}$

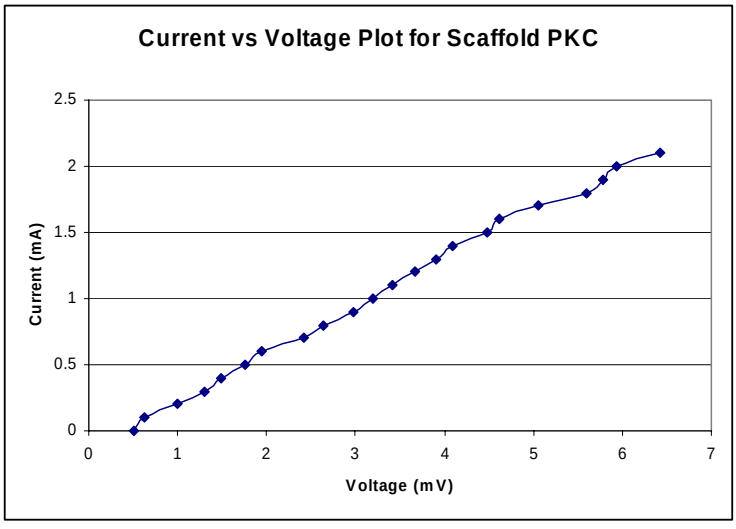

Figure 6.24. Current versus voltage plot for scaffold PKC.

Table 6.5. Conductivity values of scaffolds P, PK, PC and PKC.

Scaffold	Conductivity of Scaffold
P	$5.6 \times 10^{-8}\ \Omega^{-1}cm^{-1}$
PK	$7.13 \times 10^{-8}\Omega^{-1}cm^{-1}$
PC	$6.69 \times 10^{-4}\ \Omega^{-1}cm^{-1}$
PKC	$5.98 \times 10^{-4}\ \Omega^{-1}cm^{-1}$

The conductivity of a material is its ability to carry current (and charges). From table 6.5, we observed that the conductivity of the material increased when SWNT were incorporated into the matrix. This was an expected result as the SWNTs themselves have an electrical conductivity of 6000 $\Omega^{-1}cm^{-1}$ and their incorporation in the fiber is expected to increase the electrical conductivity of the fiber. The scaffolds containing SWNT possess only 1% of SWNT in their matrix (by weight) and this small amount of SWNT has increased the conductivity of the polymeric scaffold by four orders of magnitude. The values found for the PC and PKC scaffold puts them in the bracket of semi-conductors. The four probe tests have revealed that the numerical values of the conductivity of the scaffolds containing SWNT is close to that of the natural bone tissue.

6.2 Characterization Cell-Matrix Interactions

6.2.1. Results from ESEM

The scaffolds were seeded with human chondrocytes and imaged at various time points (10 days, 3 weeks, 6 weeks and nine weeks). The images obtained are listed below. ESEM images (fig 6.25) obtained 10 days after the cells were seeded on the scaffold revealed the presence of flat, polygonal structures that resemble chondrocytes in morphology. The images clearly show that the chondrocytes have developed an extracellular matrix that is moving all over the scaffold by means of cytoplasmic extensions (intercellular connections), guided along the fibers of the scaffold. At this stage, all four scaffolds behaved similarly.

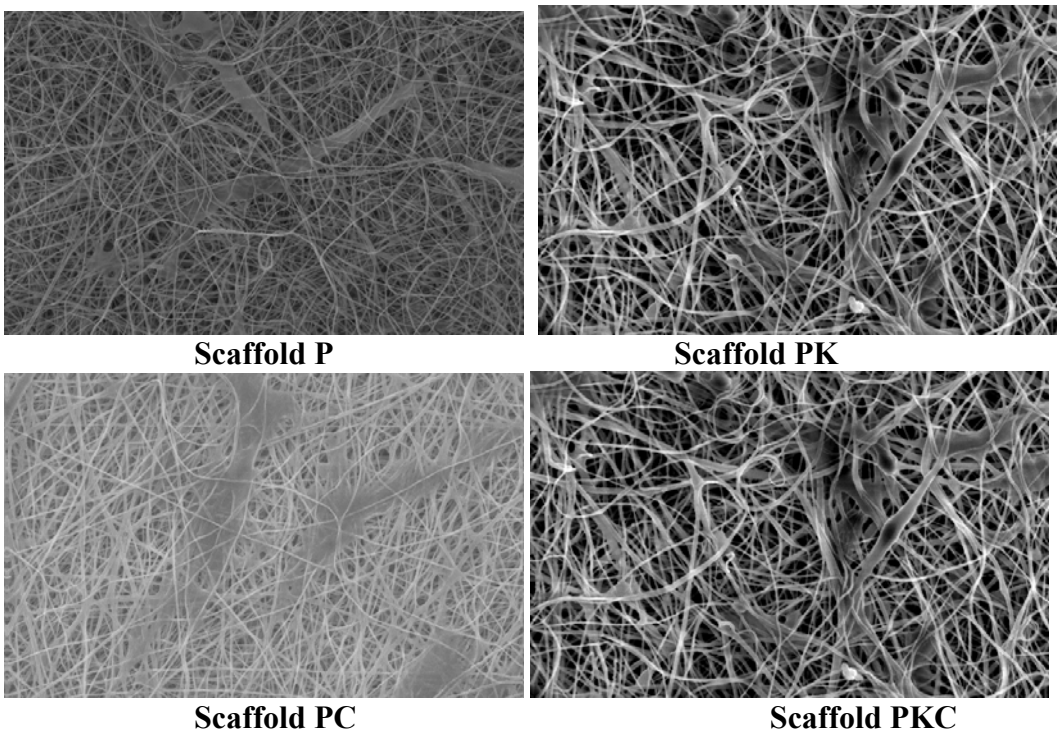

Figure 6.25. ESEM images of scaffolds P, PK, PC and PKC after 10 days of cell culturing.

ESEM images (fig 6.26) obtained 3 weeks into the *in vitro* study revealed that chondrocytes were still present on the scaffold and had begun to proliferate into the scaffold from the surface along the fibers of the polymeric matrix. The extracellular matrix of the chondrocytes appeared to be sealing off the pores. At this stage, all four scaffolds behaved similarly.

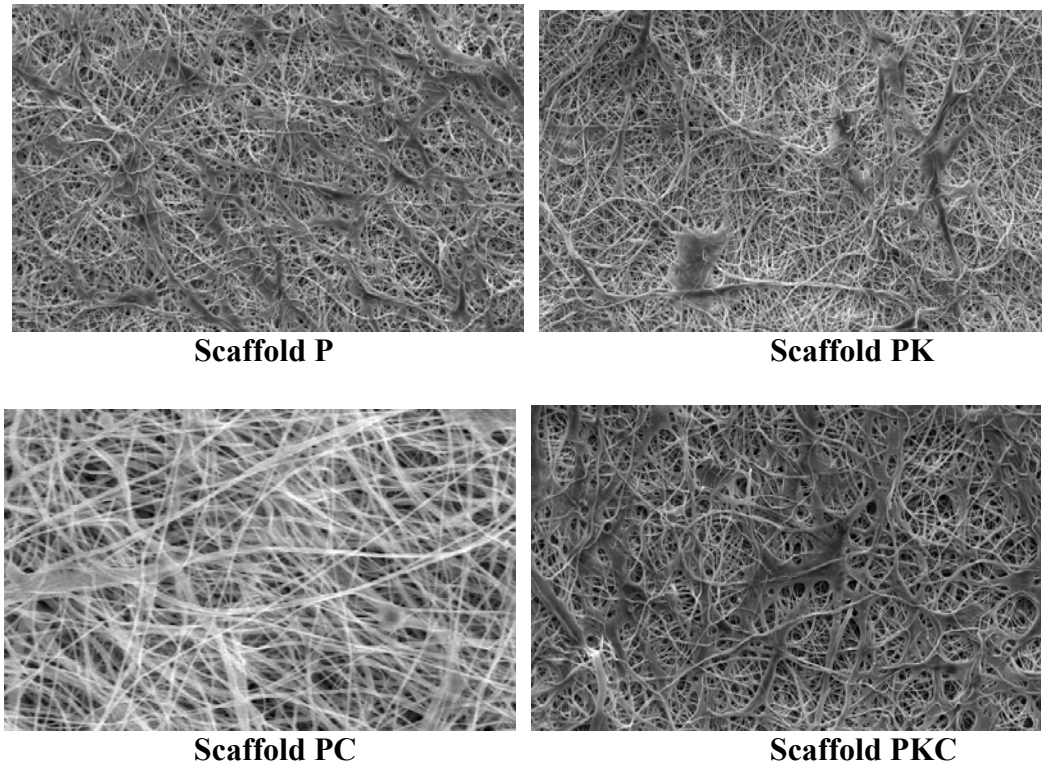

Figure 6.26. ESEM images of scaffolds P, PK, PC and PKC after 3 weeks of cell culturing.

ESEM images (fig 6.27) obtained 6 weeks into the *in vitro* study revealed that chondrocytes were still present on the scaffold. In scaffolds P, PK and PKC, the chondrocytes appeared to have covered the entire top surface of the scaffold and most pores were sealed by the extracellular matrix of the cells. Scaffold PC, however, showed a different trend. In this scaffold, the cells had not appeared to have covered the entire top surface, but there still appeared to be viable chondrocytes attempting to proliferate into the scaffold.

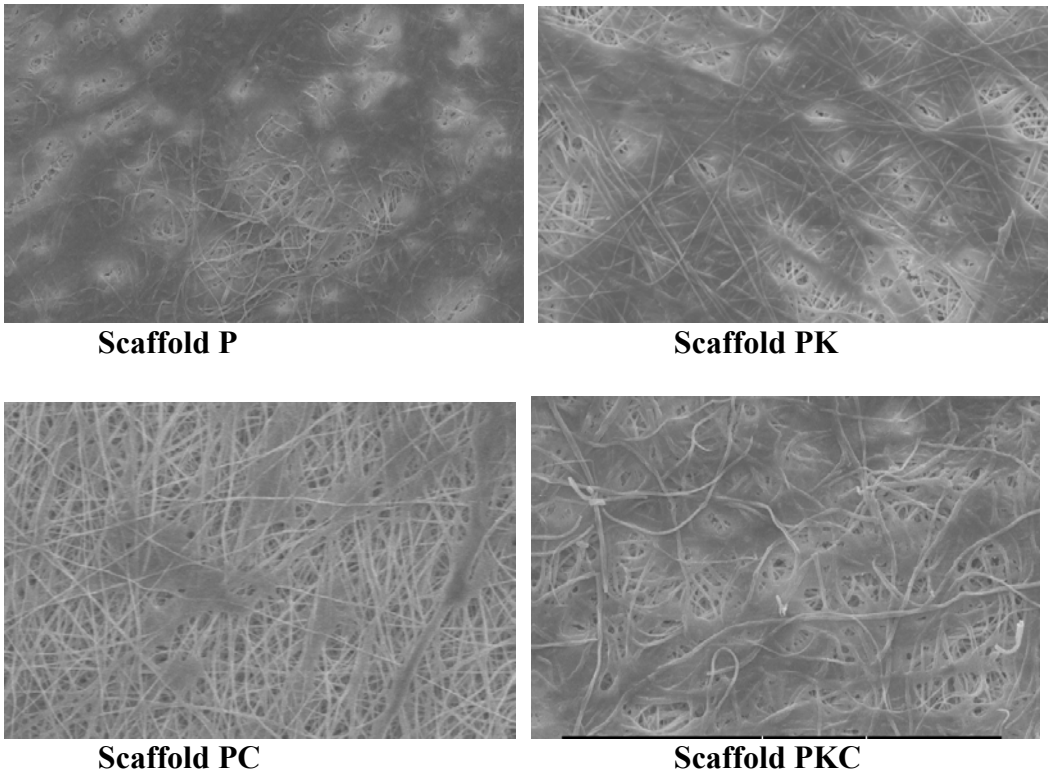

Figure 6.27. ESEM images of scaffolds P, PK, PC and PKC after 6 weeks of cell culturing.

At the end of nine weeks, the pores in the matrix appear to have been sealed off by proliferating chondrocytes and the extracellular matrix (fig 6.28). For scaffolds P, PK and PKC, the fibrous scaffold was no longer visible as it was completely covered with the cells. In scaffold PC, however, the cell attachment appears to be less than that of the other scaffolds, but viable cells exist on the scaffold even at the end of nine weeks, suggesting that SWNT do not have an adverse effect on the cell growth. Also, scaffold PKC too contains SWNT and since this scaffold interacts very well with the chondrocytes, there is no reason to believe that SWNT are toxic or have an adverse effect on chondrocytes growth and viability.

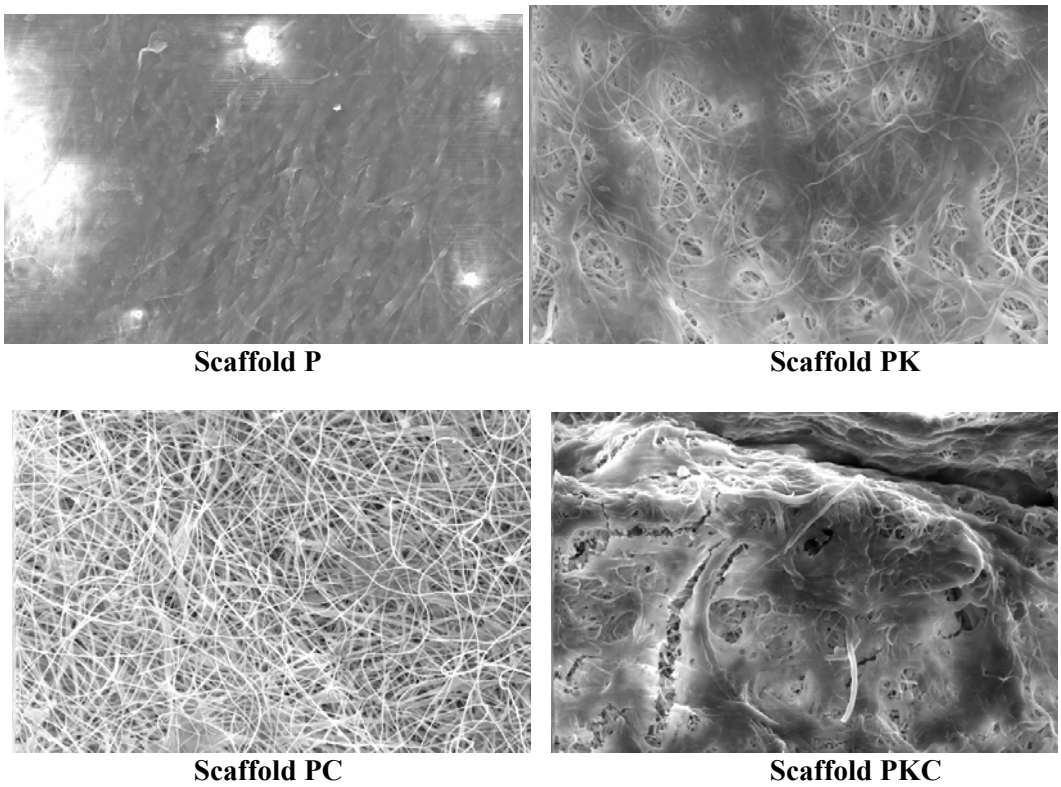

Figure 6.28. ESEM images of scaffolds P, PK, PC and PKC after 9 weeks of cell culturing.

ESEM images throughout the entire 9 weeks in vitro study have been summarized in fig 6.29. In this summary, we observed the trend of the proliferating chondrocytes on the scaffolds P, PC, PK and PKC.

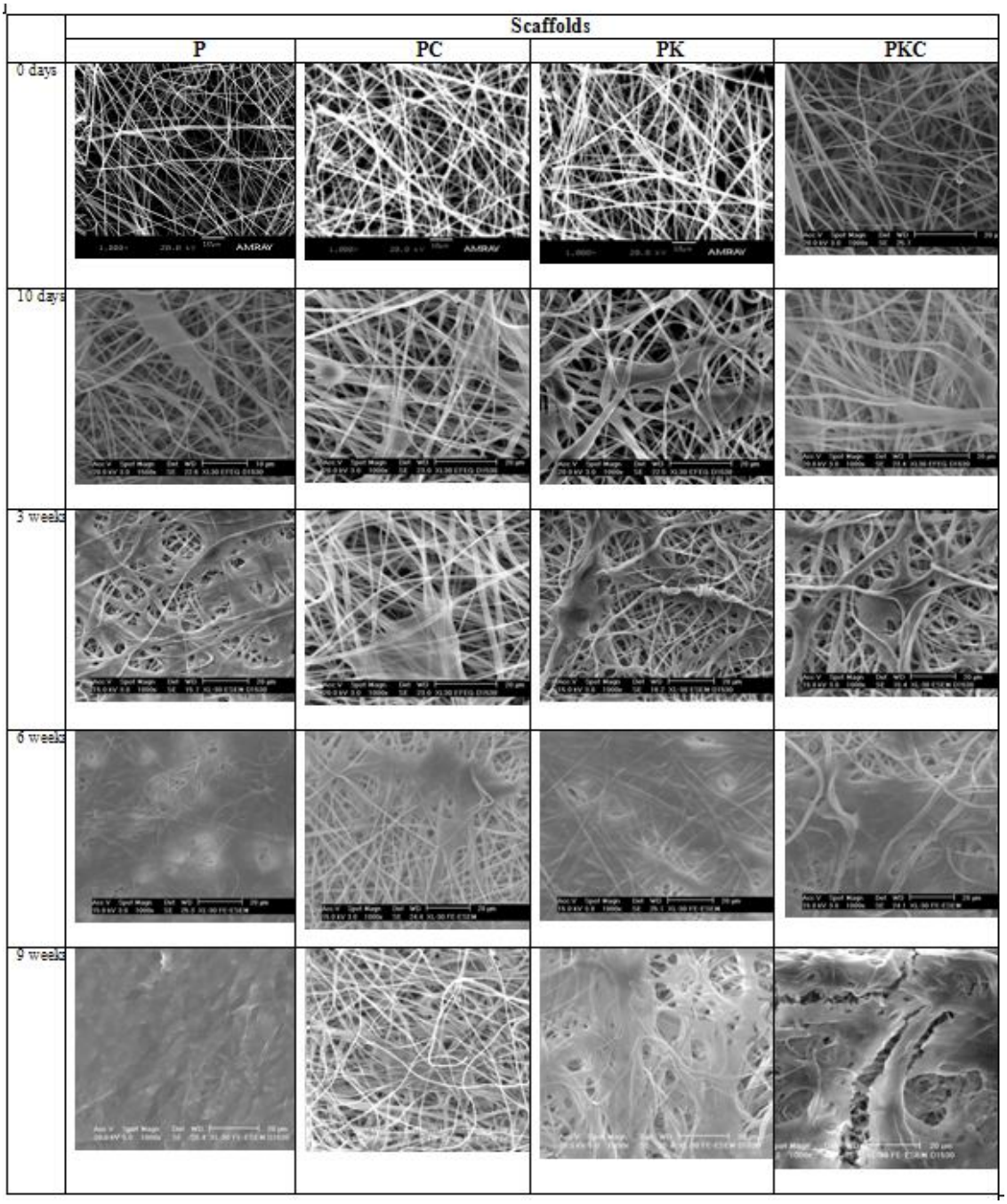

Figure 6.29. Summary of *in vitro* study over a period of 9 weeks (1000x).

6.2.2 Viability of Chondrocytes on the Scaffold

MTT assay was performed at the end of nine weeks to quantify the viable chondrocytes present on the four scaffolds. The absorbance for each scaffold was measured at 550nm and noted (Fig. 6.30). In this experiment, the absorbance is an indication of the number of viable cells present, so a high absorbance implies more viability. As can be seen, the amount of viable cells on the scaffolds containing ε-PL (PK and PKC) exceeds that of the scaffolds without it (P and PC). However, the amount of viable cells is lowest for the PC scaffold but yet, the assay detected chondrocyte viability on the PC scaffold even after 9 weeks of culture, and this is an indication that the SWNTs are not detrimental to cell-growth and viability. It implies, however, that the absence of ε-PL in the scaffold containing SWNTs may hinder the attachment of cells on the scaffold. In the presence of ε-PL the chondrocytes interact very favorably with the fibrous scaffold and cell viability on the PKC scaffold is similar to that of the PK scaffold. This substantiates the fact that if SWNTs are to be used in a tissue engineering scaffold to increase its the mechanical and electrical properties, a positively charged amino acid (such as lysine or glucosamine) should also be incorporated in the fibers.

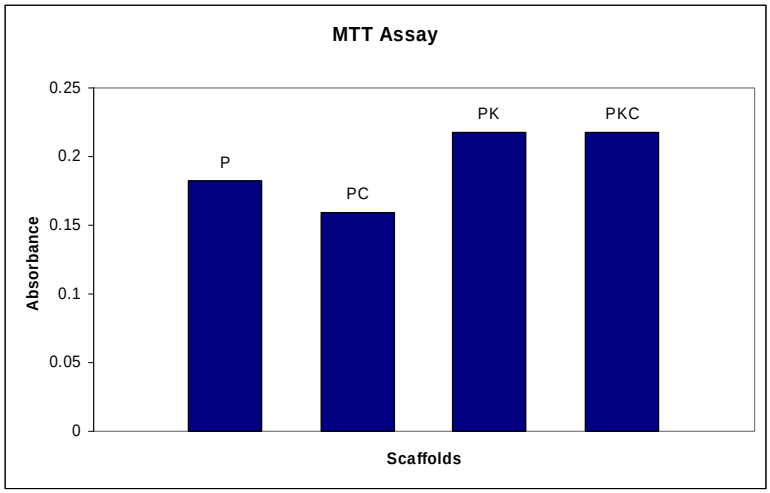

Fig. 6.30. Absorbance of scaffolds P, PC, PK and PKC after 9 weeks of culture.

CHAPTER 7: SUMMARY AND CONCLUSION

The goal of this study was to fabricate a nanofibrous polymeric scaffold, with improved mechanical and electrical properties, to be used as in the regeneration of articular cartilage. The base polymer used in this study was Poly-L-Lactic acid (PLLA). The scaffold was fabricated by means of the electrospinning technique. The feasibility of single walled carbon nanotubes as a suitable reinforcement for electrospun PLLA scaffold was studied. The effect of Poly-ε-L-Lysine (ε-PL) on the interaction of the scaffold with human chondrocytes was also studied. Four types of scaffolds were evaluated and compared in terms of their mechanical and electrical properties and their interaction with human chondrocytes. The four scaffolds evaluated in this study were:

1. PLLA (scaffold P)
2. PLLA/SWNT (scaffold PC)
3. PLLA/ ε-PL (scaffold PK)
4. PLLA/ ε-PL/SWNT (scaffold PKC)

ESEM images of the scaffolds showed that fibers containing SWNT had a rough surface morphology while ordinary polymeric fibrils displayed a smooth morphology and all fiber diameters were in the 500 nm range.

The first hypothesis was that the incorporation of SWNT in the polymeric fibrils would improve the mechanical properties. This hypothesis was tested by

subjecting the four scaffolds to mechanical tests. The results of this showed that the scaffolds containing SWNT displayed a modulus of about 125 MPa which is about 2.5 times that of the scaffolds without the reinforcement. There is also a slight increase in toughness of the reinforced scaffolds as compared to the unreinforced scaffolds. The four probe conductivity test of the scaffolds revealed that PC and PKC were in the semi-conductor range with their electrical conductivity approximately 10000 times higher than that of the P and PK.

The second hypothesis was that the SWNT could be aligned along the fiber diameter by electrospinning. This hypothesis was validated by subjecting the electrospun scaffolds to Raman spectroscopy and transmission electron microscopy. The Raman spectra of fibers in the PC and PKC scaffolds (fig. 6.15) provide strong evidence of the presence of SWNT in them as the spectra is identical to known spectra of SWNTs[84]. Essentially, co-electrospinning of the polymer and SWNT resulted in incorporation of the SWNT within the polymeric fibril. TEM (fig. 6.11 and fig.6.14) further confirms the presence of SWNT in the PC and PKC scaffolds as well as their alignment along the fiber orientation. The increase in mechanical properties of the scaffolds reinforced with SWNT can be attributed to the alignment of SWNT along the fibers.

The third hypothesis was that the nanofibrous structure of the electrospun scaffolds would aid in cell attachment and proliferation. This hypothesis was evaluated by coating the scaffolds with collagen and seeding them with human

chondrocytes. The scaffolds were imaged at various time points (10 days, 3 weeks, 6 weeks and 9 weeks). This study revealed that the cells proliferated through the scaffold by means of cytoplasmic extensions that were guided along the fibers. The random fibrous electrospun scaffold coated with collagen mimics the actual *in vivo* extracellular matrix of cartilage tissue and facilitates cell growth. The MTT assay revealed the presence of viable cells on all four scaffolds at the end of nine weeks.

The fourth hypothesis was that incorporation of ε-PL in the fibers would improve their interaction with the chondrocytes. The ESEM images as well as the MTT assay from the *in vitro* study of the scaffolds revealed that chondrocytes interacted better with scaffolds containing ε-PL. The fact that the combination scaffold of Poly-L-lactic acid, SWNT and ε-PL (PKC) interacted very well with the chondrocytes during the cell culture studies proves that SWNT do not have an adverse effect on the viability of the chondrocytes. However, it may prove to hinder in cell attachment when used alone. The advantage of using SWNT is that it increases the mechanical and electrical properties significantly and so, in order to incorporate SWNT in a tissue engineered scaffold, ε-PL should also be incorporated in the fibrous matrix.

Further work needs to be carried out in this area to assess the actual behavior of the scaffold at the implant site. This can be done by *in vivo* study. Also, the mechanical properties of the scaffolds can be further increased by achieving

better dispersion of SWNT in the polymeric spinning dope. As lysine is a polar, hydrophilic positively charged amino acid, this study could be repeated using another amino acid with similar properties.

The main challenge in applying biomaterials to regeneration of tissues is the failure at the implant interface. This is particularly relevant in cartilage regeneration as the tissue has limited capacity for self repair. There are also no studies that compare the repair of the natural tissue to that of other forms. Long-term functional outcome of any composite scaffold is still unknown as most of them are still in the developmental stages.

To conclude, the electrospinning process may be used to fabricate a three dimensional, fibrous, nano-composite matrix to facilitate cartilage regeneration. This matrix is highly porous and provides adequate space for the chondrocytes to reside in. The fibrous nature of the scaffold aids the cells seeded on it to attach as well as proliferate along the fibers. Incorporation of SWNT improved the physical properties of the scaffolds and incorporation of ε-PL improved the cell interaction with the scaffolds. With proper in vivo test and verification, the strategy of a 3-D PLLA/CNT/PL/collagen II nanocomposite fibrous scaffold system may be promising for the formation of a family of scaffolds for cartilage tissue regeneration.

LIST OF REFERENCES

1. The Biomedical Engineering Handbook: Second Edition; CRC Pess LLC; 2000.

2. Buckwalter, J.A. Chondral and osteochondral injuries: mechanisms of injury and repair responses. Oper. Tech. Orthop.1997; 7: 263.

3. Slivka, M, Leatherbury NC, Kieswetter K, Nienderauer GG. Porous, Resorbable, Fiber-Reinforced Scaffolds Tailored for Articular Cartilage Repair. Tissue Engineering 2001, 7(6), 767-80

4. Jackson D, Scheer M, Simon T. Cartilage Substitues: Overview of Basic Science and Treatment Options; J Am Acad Orthop Surg 2001;9:37-52

5. Gray H, (1821–1865). Anatomy of the Human Body. 1918.

6. Wu JZ, Herzog W. Elastic anisotropy of articular cartilage is associated with the microstructures of collagen fibers and chondrocytes. J Biomech. 2002 ; 35(7): 931-42.

7. Mow VC, Hayes WC. Basic Orthopaedic. Biomechanics 1991; Chapters: “Structure and Function of Articular Cartilage and Meniscus,"

8. Maroudas A. Physicochemical properties of articular cartilage. Adult Articular Cartilage 1979; Pitman Medical Publishing: 215-290

9. Buckwalter JA, Mankin HJ. Articular cartilage: tissue design and chondrocyte-matrix interactions. AAOS Inst Course Lect 1998;47:477-86.

10. Mow VC, Proctor CS, Kelly MA. Biomechanics of articular cartilage, Basic Biomechanics of the Musculoskeletal System 2nd ed. Lea and Febiger 1989; 2nd edition: 32

11. Edwards, J. Physical Characteristics of Articular Cartilage. Proc Inst Mech Engrs 1967;181(3J):16-24

12. Edwards J, Smith AU. The uptake of fluid by living cartilage after compression. J Physiol 1966; 183: 5-6

13. Maroudas A, Schneiderman R. Free and exchangeable or trapped and non-exchangeable water in cartilage. J Orthop Res 1987; 5: 133-8

14. Buckwalter JA. Articular cartilage. AAOS Inst Course Lect 1983;32:349-70

15. Armstrong CG, Mow VC. Variations in the intrinsic mechanical properties of human articular cartilage with age, degeneration and water content. J Bone Joint Surg 1982; 106: 165-73

16. Hutmacher DW. Scaffolds in tissue engineering bone and cartilage. Biomaterials 2000; 21(24); 2529-43.

17. E. B. Hunziker. Articular cartilage repair: basic science and clinical progress. A review of the current status and prospects. Osteoarthritis and Cartilage 2001; 10: 432–63

18. Howell DS. Pathogenesis of osteoarthritis. Am J Med 1986;80:24–8.

19. Hunziker EB. Articular cartilage repair: are the intrinsic biological constraints undermining this process insuperable? Osteoarthr Cartil 1999;7:15-28.

20. Hunziker EB, Kap"nger E. Removal of proteoglycans from the surface of defects in articular cartilage transiently enhances coverage by repair cells. J Bone Jt Surg 1998;80-B:144-50.

21. Shapiro F, Koide S, Glimcher MJ. Cell origin and differentiation in the repair of full-thickness defects of articular cartilage. J Bone Joint Surg 1993;75A: 532–53.

22. Tew S, Kwan APL, Hann A, Thomson B, Archer CW. The reactions of articular cartilage to experimental wounding: role of apoptosis. Arthritis Rheum 2000; 43: 215–25.

23. Gilbert JE. Am J Knee Surg. Current treatment options for the restoration of articular cartilage 1998 Winter;11(1):42-6.

24. Tissue-engineered cartilage by in vivo culturing of chondrocytes in PLGA–collagen hybrid sponge

25. C. A. Vacanti and A.G. Mikos. Tissue Engineering 1995, 1: 1

26. Langer R, Vacanti JP. Tissue engineering. Science 1993; 260:920–6.

27. Stock UA, Vacanti JP. Tissue engineering: Current State and Prospects. Annu Rev Med 2001; 52:443–51.

28. Skalak R, Fox CF. Tissue engineering. Ann Biomed Eng 1991; 19:529–33

29. Huynh T, Abraham G, Murray J, Remodeling of an acellular collagen graft into a physiologically responsive neovessel. Nat Biotech 1999; 17(11):1083–6

30. Chen G, Ushida T, Tatsuya T. Development of biodegradable porous scaffolds for tissue engineering. Material Sci Eng 2001; C (17): 63–9.

31. Park JB, Bronzino JD. Biomaterials: Principles and applications. CRC Press 2003; 55-115

32. Peter SJ, Miller MJ, Yasko AW, Yaszemski MJ, Mikos AG. Polymer concepts in tissue engineering. J Biomed Mater Res 1998; 43: 422–7.

33. Thomson RC, Yaszemski MJ, Powers MJ, Mikos AG. Fabrication of Biodegradable polymer scaffolds to engineer trabecular bone. J Biomater Sci Polym Ed 1995; 7: 23–38.

34. Freed LE, Vunjak-Novakovic G, Biron RJ, Eagles DB, Lesnoy DC, Barlow SK, Langer R. Biodegradable polymer scaffolds for tissue engineering. Biotechnology 1994; 12: 689–93.

35. Tatsuya T, Chen G, Ushida T. Biodegradable porous scaffolds for tissue engineering. J Artif Organs 2002; 5: 77– 83.

36. Chen G, Sato T, Ushida T, Hirochika R, Ochiai N, Tateishi T. Regeneration of cartilage tissue by combination of canine chondrocyte and a hybrid mesh scaffold. Materials Science and Engineering 2004.

37. Sittinger M, Reitzel D, Dauner M, Hierlemann H, Hammer C, Kastenbauer E, Planck H, Burmester GR, Bujia J. Resorbable polyesters in cartilage engineering: affinity and biocompatibility of polymer fiber structures to chondrocytes. J Biomed Mater Res 1996; 33(2): 57-63.

38. Mikos AG, Thorsen AJ, Czerwonka LA. Preparation and characterization of poly(L-lactic acid) foams. Polymer 1994; 35: 1068-77.

39. Mikos AG, Sarakinos G, Leite SM. Laminated three-dimensional biodegradable foams for use in tissue engineering. Biomater 1993; 14: 323-30

40. Gooch KJ, Kwon JH, Blunk T, Langer R, Freed LE, Vunjak-Novakovic G. Effects of mixing intensity on tissue-engineered cartilage. Biotechnol Bioeng 2001; 20; 72(4): 402-7.

41. Washburn NR, Simon CG Jr, Tona A, Elgendy HM, Karim A, Amis EJ. Co-extrusion of biocompatible polymers for scaffolds with co-continuous morphology. J Biomed Mater Res 2002 ; 60(1): 20-9.

42. Lanza RP, Langer R, Chick WL. Principles of tissue engineering. Academic press 1996; 273-93.

43. Agrawal CM, Ray RB. Biodegradable polymeric scaffolds for musculoskeletal tissue engineering. J Biomed Mater Res 2001; 55(2):141-50.

44. Li W, Laurencin CT, Caterson EJ, Tuan RS, Ko FK. Electrospun nanofibrous structure: A novel scaffold for tissue engineering. J Biomed Mater Res 2002; 60: 613–21.

45. Ko F, Gogotsi Y, Ali A, Naguib N, Ye H, Yang G.L, Li C, Willis P. Electrospinning of Continuous Carbon Nanotube-Filled Nanofiber Yarns, Advanced Materials 2003; 15(14): 1158-61.

46. Cameron JR, Skofronick JG, Grant RM. Physics of the Body 1999. Medical Physics Publishing.

47. Nimmagadda A, McFetridge P. Single walled carbon nanotubes: An assessment of biocompatibility for tissue engineering. Cardio Path 2004; 13: S80-138.

48. Ko FK, Khan S, Ali A, Gogotsi Y, Naguib N, Yang G, Li C. Structure and properties of carbon nanotubes reinforced nanocomposites. American institute of aeronautics and astronautics 2002-1426.

49. Ko FK, Borden MD, Laurencin CT. The role of fiber architecture in biocomposites: The tissue engineering approach. Proceedings of ICCM 13, Beijing, June 25-28, 2001

50. Ma PX, Langer R. Morphology and mechanical function of long term in vitro engineered cartilage. J Biomed Mater Res 1999; 44: 217-21.

51. Li WJ, Laurencin CT, Caterson EJ, Tuan RS, Ko FK. Electrospun nanofibrous structure: A novel scaffold for tissue engineering. J Biomed Mater Res 2002; 60: 613-21.

52. Riesle J, Hollander AP, Langer R, Freed LE, Vunjak-Novakovic G. Collagen in tissue-engineered cartilage: Types, structure, and crosslinks. J Cell Biochem 1998; 71:313–27.

53. Satoa T, Chen G, Ushidad T, Ishiia T, Ochiaia N, Tateishib T, Tanaka J. Evaluation of PLLA–collagen hybrid sponge as a scaffold for cartilage tissue engineering. Mat Sci Eng C 2004

54. Ishikawa H, Fudetani S, Hirohashi M. Mechanical properties of thin films measured by nanoindenters, Appl Surf Sci 2001; 178: 56- 42.

55. Kracke B, Damaschke B. Measurement of nanohardness and nanoelasticity of thin gold films with scanning force microscope, Appl Phys Lett 2000; 77: 361-63.

56. de Pablo PJ, Martınez MT, Colchero J, Gomez-Herrero J, Maser WK, de Benito AM, Munoz E, Baro AM, Electrical characterization of single-walled carbon nanotubes with Scanning Force Microscopy, Mater Sci Eng 2001; C15: 149–51.

57. Hertel T, Martel R, Avouris P. Manipulation of Individual Carbon Nanotubes and Their Interaction with Surfaces. J Phys Chem 1998; B 102: 910-5.

58. Supronowicz PR, Ajayan PM, Ullmann KR, Arulanandam BP, Metzger DW, Bizios R. Novel current conducting composite substrate for exposing osteoblasts to alternating current stimulation. J of Biomed Mater Res 2001; 49: 499-506.

59. Treacy MMJ, Ebbesen TW, Gibson JM. Exceptionally high Young's modulus observed individual carbon nanotubes. Nature 1196; 381: 678-80.

60. Iijima S, Ichihashi T. Single-shell carbon nanotubes of 1-nm diameter. Nature 1993; 363:603.

61. Bethune DS, Kiang CH, de Vries MS, Gorman G, Savoy R, Vasquez J, Beyers R. Cobalt-catalysed growth of carbon nanotubes with single-atomic-layer walls. Nature 1993; 363:605.

62. Harris, PJF. Carbon nanotubes and related structure: new materials for the twenty-first century. Cambridge university press 1999; 1-210.

63. Dresselhaus M, Dresselhaus G, Eklund P. Science of Fullerenes and Carbon Nanotubes. Academic Press 1996; New York.

64. Cooper CA, Ravich D, Lips D, Mayer J, Wagner HD. Distribution and alignment of carbon nanotubes and nanofinrils in a polymer matrix. Comp Sci Tech 2002; 62: 1105-12

65. Biercuk MJ, Llaguno MC, Radosvljevic M, Hyun JK, Johnson AT. Carbon nanotube composites for thermal management. Appl Phys Lett 2002;80:15.

66. Ounaies Z, Park C, Wise KE, Siochi EJ, Harrison JS. Electrical properties of single wall carbon nanotube reinforced polyimide composites. Compos Sci Technol 2003; 63:1637–46.

67. Andrews R, Weisenberger MC. Carbon nanotube polymer composites. Current Opin Sol St Mat Sci 2003.

68. Thostenson EL, Ren Z, Chou T, Composites Science and Technology, , Advances in the science and technology of carbon nanotubes and their composites: a review, 2001. 1899-1912.

69. Weisenberger MC, Grulke EA, Jacques D, Rantell T, Andrews R. Enhanced mechanical properties of polyacrylonitrile/multiwall carbon nanotube composite fibers. J Nanosci Nanotech 2003;3(6),

70. Dalton AB, Collins S, Munoz E, Razal JM, Ebron VH, Ferraris JP. Super-tough carbon-nanotube fibres. Nature 2003;423:703.

71. Mickelson ET, Huffman CB, Ringlet AG, Smalley RE, Hague RH, Margrave JL. Fluorination of single-wall carbon nanotubes. Chem Phys Let 1998; 296: 188–94.

72. McCArthy B, Coleman JN, Czerw R. A microscopic and spectroscopic study of interactions between carbon nanotubes and a conjugated polymer. J Phys Chem B 2002; 106: 2210-6.

73. Nimmagadda A, McFetridge P. Single walled carbon nanotubes: An assessment of biocompatibility for tissue engineering. Cardio Path 2004; 13: S80-138.

74. Formhals A. U.S. Patent, 1,975,504; 1934.

75. Reneker DH, Chun I. Nanotechnology 1996; 7:216

76. Jaeger R, Bershoef MM, Batle CM, Schonherr H, Vancso GJ. Macromol Symp 1998; 127:141

77. Jin HJ, Fridrikh SV, Rutledge GC, Kaplan DL. Biomacromolecules 2002;3:1233–9.

78. Huang ZM, Zhang YG, Kotaki M, Ramakrishna S. A review on polymer nanofibers by electrospinning and their applications in nanocomposites. Comp Sci Tech 2003; 63:

79. Zheng J, Northrup SR, Hornsby PJ. Modification of materials formed from poly(L-lactic acid) to enable covalent binding of biopolymers: application to high-density three-dimensional cell culture in foams with attached collagen. In Vitro Cell Dev Biol Anim 1998;34:679–84.

80. Pelletier MJ. Analytical applications of raman spectroscopy. Blackwell science 1999; 414-25.

81. Duesberg GS,Loa I, Burghard M, Syassen K, Roth S. Polarized Raman Spectroscopy on Isolated Single-Wall Carbon Nanotubes. Physical Review Letters 2000; 85; 25: 5436

82. Weber WH, Merlin R. Raman Scattering in Materials Science. Springer-Verlag Berlin Heildberg 2000.

83. Weber W, Merlin R. Raman Scattering in Materials Science. Springer Berlin 2000.

84. Pelletier MJ, Analytical applications of Raman Spectroscopy, Blackwell science, 1999; 418-425

APPENDIX A: DATA FROM THE FOUR PROBE CONDUCTIVITY TEST

Table A1. Conductivity test data for the silicon wafer

Current (mA)	Voltage (mV)
0	6.2
0.1	21.3
0.2	38.14
0.3	53.8
0.4	69.25
0.5	85.2
0.6	100.3
0.7	115.17
0.8	132.1
0.9	147
1	164.6
1.1	179.28
1.2	195
1.3	211
1.4	226.4
1.5	242.4
1.6	258
1.7	272.5

Table A2. Conductivity test data for scaffold P

Current (mA)	Voltage (mV)
0	6.7
0.1	21.75
0.2	38
0.3	54.5
0.4	70.75
0.5	87.6
0.6	102.8
0.7	119.4
0.8	135.6
0.9	151.44
1	167.3
1.1	181.2
1.2	198.7
1.3	215.7
1.4	231.4
1.5	246
1.6	265.2
1.7	280.5
1.8	298.8
1.9	314.7
2	330.6
2.1	344.3

Table A3. Conductivity test data for scaffold PK

Current (mA)	Voltage (mV)
0	6.1
0.1	21.62
0.2	37.41
0.3	52.88
0.4	68.42
0.5	85.7
0.6	99.18
0.7	116.28
0.8	130.02
0.9	146.71
1	162.91
1.1	178.03
1.2	198.27
1.3	209.49
1.4	228.3
1.5	240.34
1.6	255.2
1.7	271.5
1.8	286.8
1.9	302.7
2	318.6
2.1	333.3

Table A4. Conductivity test data for scaffold PC

Current (mA)	Voltage (mV)
0	0.8
0.1	0.935
0.2	1.11
0.3	1.42
0.4	1.62
0.5	2.01
0.6	2.16
0.7	2.46
0.8	2.78
0.9	3.01
1	3.24
1.1	3.28
1.2	3.76
1.3	3.97
1.4	4.05
1.5	4.56
1.6	4.69
1.7	4.94
1.8	5.16
1.9	5.49
2	5.73
2.1	5.85

Table A5. Conductivity test data for scaffold PKC

Current (mA)	Voltage (mV)
0	0.5
0.1	0.63
0.2	0.99
0.3	1.31
0.4	1.48
0.5	1.75
0.6	1.94
0.7	2.42
0.8	2.63
0.9	2.98
1	3.19
1.1	3.41
1.2	3.67
1.3	3.91
1.4	4.09
1.5	4.48
1.6	4.61
1.7	5.06
1.8	5.6
1.9	5.79
2	5.94
2.1	6.42